Bioengineering functional polymer systems for glycan-based targeting and drug release

Elaine Sze Limqueco

A thesis

submitted in partial fulfillment of the

requirements for the degree of

Masters of Science in Bioengineering

University of Washington

2024

Committee:

Daniel M. Ratner

Eoin West

Program authorized to to offer Degree:

Bioengineering

University of Washington

Bioengineering functional polymer systems for glycan-based targeting and drug release

Elaine Limqueco

Chair of the Supervisory Committee: Professor Daniel M. Ratner

Abstract

Bioengineering drug delivery facilitates re-potentiation of existing drugs and drug candidates, bypassing hurdles in novel drug development and accelerating the advance of medicine. Drug delivery strategies aim to enhance therapeutic effect by enhancing delivery to the target cells or tissues, while curtailing adverse off-target effects. Existing approaches include liposomes, polymeric miscelle, protein-based nanoparticles, antibody-drug conjugates, dendrimers, and polymer drug conjugates. These systems provide the framework for the addition of additional functionalities, including modalities enabling targeting or controlled drug release. This thesis describes two projects utilizing the same RAFT-based polymerization strategy to synthesize polymer-drug conjugates, incorporating different modalities to enable glycan-based targeting to the *Pseudomonas a.* biofilm and to extend drug release within polymer-drug conjugate manufactured into nanofibers.

Keyword: Drug Delivery, Polymer, Drugamer, Tenofovir, Nano-fiber, Drug release, Carbohydrate Targeting, Pseudomonas, Biofilm

Table of Contents

List of Figures

1 List of Tables

1 Introduction

1.1 Hurdles in modern medicine

Some of the greatest modern medical challenges lay in the development of solutions for medication nonadherence and treating “undruggable” diseases, where effective doses of current drugs cannot reach therapeutic targets. By re-engineering the delivery method of pharmaceutical compounds, we create a multimodal opportunity to address these issues and enhance therapeutic performance.

1.1.1 Combatting medication non-adherence

Nonadherence in treatment of chronic disease is an complex issue, influenced by, amongst many other factors, socio-economic status, inadequate or fragmented care, complicated treatment regimes, cognitive impairment, “pill-fatigue”, forgetfulness, and depression[1]. This is of great concern in many diseases, including schizophrenia, diabetes, and infections. By developing therapies which reduce patient burden in continuing treatment, we can greatly improve not only health but more importantly, quality of life. Two promising options are to engineer extended release drugs or to pursue alternative delivery methods.

1.1.1.1 Extended release drugs

Reducing dosing frequency and simplifying dosing schedules greatly improve medication adherence and patient health. These Extended release anti-psychotics have similarly

improved patient health, functionality, stability, and quality of life1–3. Similarly, insulin delivery pens and automated insulin delivery devices have greatly improved target time in range of glucose levels and improved quality of life, demonstrating significant efficacy in improving health and compliance6–8. Reducing the number of doses patients must take obviates many of the contributors to nonadherence. This is of significant concern in the treatment of infections, where poor medication adherence risks not only reinfection but potentially transmitting the infection and contributing to the development of antibiotic resistance.

1.1.1.2 Alternate delivery methods

In many medication settings, such as the treatment of schizophrenia and HIV, the only extended release options are injectable medications. Administration through needles precludes these extended release medications for many groups due to psychological challenges. In addition to the ubiquitous needle-phobia, many may have aversions to injectable extended release medications due to concerns about control—such as the irreversibility after injection—and negative associations with drug usage, especially for patients with prior history of drug use or who are in the process of recovery from drug abuse[7]. Consequently, development of alternative administration methods is critical in the reduction medication nonadherence.

1.1.2 Targeting “undruggable” diseases

Most medications are non-targeted and administered systemically. This lack of specificity translates to needing higher dosages to reach the intended target organ or tissue, increasing the risk of off-target effects and adverse reactions deleterious to the health and well-being of patients[8]. If a drug cannot efficiently reach or treat the targeted organ, higher dosages and more extensive and prolonged therapies may be required for complete rehabilitation. These increased dosages translate to higher medical costs, decreasing the accessibility of the therapy. More significantly, untargeted medications frequently show poor efficacy in the treatment of "undruggable" diseases—such as solid tumor cancers, Alzheimer's, multiple sclerosis, cystic fibrosis, and pulmonary infections—where access to the targeted organ or tissue is barred by physiological barriers including the extracellular matrix, blood-brain barrier, mucosal barriers, and the cellular membrane[9]. By engineering targeting properties into medications, treatment can overcome these limitations. In the advancement of cancer treatment, targeted treatment has become pivotal in increasing patient survival, health, and quality of life[10–12].

1.2 Pro-drug polymers

Pro-drugs have become an entrenched strategy to overcome barriers for otherwise promising drug candidates, overcoming challenges such as chemical instability, toxicity, low aqueous solubility, short half-lives, and physiological barriers to therapeutic targets [13].

Conventional pro-drug strategies alter administration, distribution, metabolism, and excretion (ADME). With the polymer chemistry and synthetic methods used in **pro-drug containing polymer (drugamer)** formulation allow for precise control and improvement of many drug properties, such as targeting, solubility, retention, and biocompatibility.

1.2.1 Modularity

The use of drugamers represents a modular opportunity for versatile selection and combination of varying monomers. Many synthetic methods pro-drug polymers now utilize **Reversible addition-fragmentation chain transfer (RAFT)** polymerization. Since it was first reported in 1988, RAFT has become one of the most popularly used methods of controlled radical polymerization[14]. It permits exhaustive control of molecular weight, DP, polydispersity, and structure, synthesizing complex polymer architectures far beyond the basic linear block copolymer, such as star, dendrimer, brush, comb-like, and cross-linked networks. More significantly, RAFT functions across a wide temperature range and is tolerant of many monomer and solvent functionalities, including aqueous solutions[15]. As a result, different moieties, linkers, and monomers can be combined and recombined to

synthesize drugamers of varying polymer compositions, yielding a repertoire with a wide range of attributes and functionality.

Figure 1: Ciprofloxacin drugamer composition

Ciprofloxacin pro-drug monomers with various linkers were polymerized with carbohydrate monomers to form ciprofloxacin pro-drug monomers discussed later in this thesis.

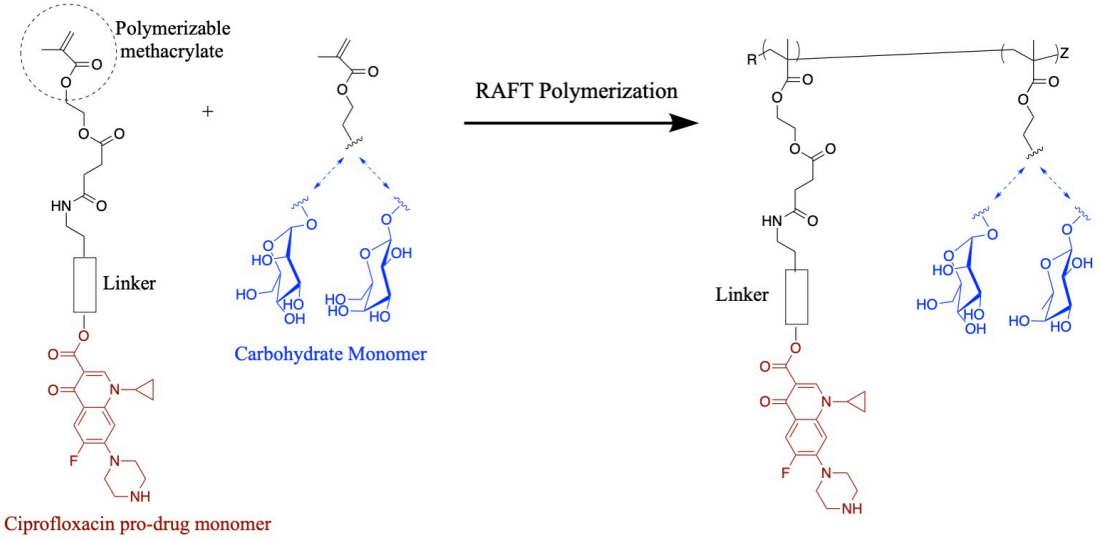

The Ratner and Stayton labs previously synthesized a series of ciprofloxacin drugamers, comprising of a ciprofloxacin pro-drug monomer and a carbohydrate monomer illustrated in Figure . Other monomers, such as fluorescent monomers for imaging purposes, were occasionally integrated.[16–19].

The ability to interchangeably incorporate different monomers within the RAFT polymerization allows for detailed analysis and comparisons. By altering the linkers between the pro-moiety and the ciprofloxacin, different release profiles can be generated and compared. Similarly, by altering the carbohydrate monomer, experiments can be performed to understand method of action and specificity.

Similarly, other modalities can be incorporated with the addition of other monomers. As seen in Figure 2, a fluorescent variant of the ciprofloxacin drugamer, synthesized through the addition of a rhodamine monomer, enabled visualization of drugamer location and retention within tissue and cells[17]. With RAFT polymerizations, other modalities be easily added to create new properties in drugamers.

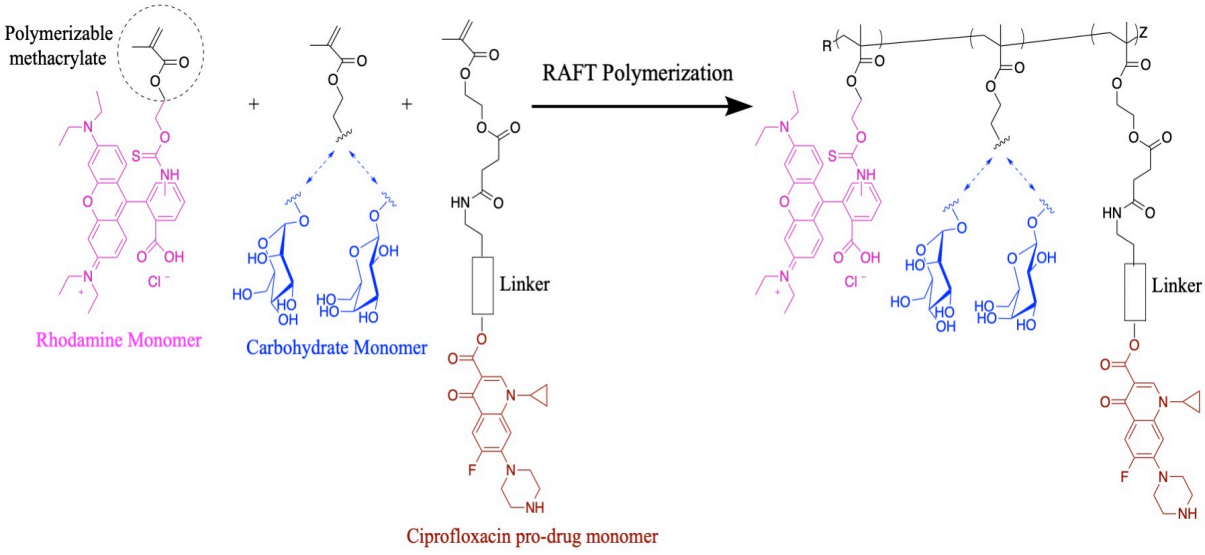

Figure 2: Schema of fluorescent ciprofloxacin drugamer polymerization

Rhodamine monomers were polymerized with varying carbohydrate monomers and ciprofloxacin pro-drug monomers with different linkers to enable visualization of the drugamers[19]

1.2.2 Targeted drug delivery

Targeting modalities are one of the most prominent features of new drug. Most cancer therapies are now targeted, utilizing ….to targeted at specific cancerous cells and tissues. As discussed earlier in section 1.1.2 Targeting “undruggable” diseases, targeted therapies improve patient health, quality of life, and outcome by reducing off target effects and

increasing efficacy at the therapeutic target, through increased concentrations delivered to the target or by escorting the drug across otherwise limiting barriers. For the purpose of illustrating targeted drug delivery with drugamers, we will focus on ciprofloxacin drugamers in the cute pulmonary lung infection setting.

Acute pulmonary infections are the third leading cause of death in the world. While many antibiotics have been developed, treatment of lung infections typically necessitate systemic therapy because antibiotics delivered as aerosols are quickly cleared from the lung tissue into the blood. Additionally, many of the most challenging pathogens evade antibiotic treatment and immune detection through the construction of biofilms, as in the case of *Pseudomonas,* or by sheltering inside alveolar macrophages, as with the causative agents of Melioidosis and Tularemia, *Burkholderia* and *Franciscella*. We exploited the alveolar macrophages' expression of the mannose receptor CD 206 to specifically target alveolar macrophages and deliver antibiotics to the intracellular bacteria.[20].

As illustrated in Figures 1-2 , multiple ciprofloxacin drugamer variants were synthesized. To evaluate the efficacy of targeting with mannose, two drugamer variants were synthesized, one expressing mannose and the other expressing the almost chemically identical carbohydrate galactose. When cultured alveolar macrophages (MPI) were incubated with the either the mannose drugamer (Man-drugamer) or the control polymers galactose drugamer (Gal-drugamer) of CBM drugamer (CBM-drugamer), shown in Figure 3a, there is markedly increased uptake of the Man-polymer than either of the control polymers. In a competition assay, MPI and HeLa cells were both dosed with mannan and galactose (Fig 3b,3c). The CD206 receptors on the MPI cells were blocked by treatment with mannan, but not with

galactose, indicating that the CD206 is very specific for mannose. (Figure 3b). As HeLa cells do not express the CD206 mannose receptor, treatment with the mannan inhibitor resulted in no significant difference in drugamer uptake (Figure 3c). To verify the specificity of the polymer targeting, MPI cells incubated with the mannan inhibitor and then dosed with drugamer resulted in inhibition of uptake only with Man-drugamer but not the Gal-polymer or CBM-polymer (Figure 3d)[16].

Figure 3. *In vitro* characterization of polymeric prodrug targeting and uptake.

A) Uptake by MPI cells treated with 1 μM of fluorescent drugamers Man-drugamer [poly(Man-co-Cipro)], Gal-drugamer [poly(Gal-co-Cipro)], and CBM-drugamer [poly(CBM-co-Cipro)]. Competition assay using CD206 and non-specific competitive inhibitors, mannan (4mg/ml) and galactose in **(B)** MPI macrophage and **(C)** HeLa cells. **(D)** MPI cells incubated with 4mg ml^{-1} mannan and dosed with non-specific control drugamers, Gal-drugamer and CBM-drugamer [16]

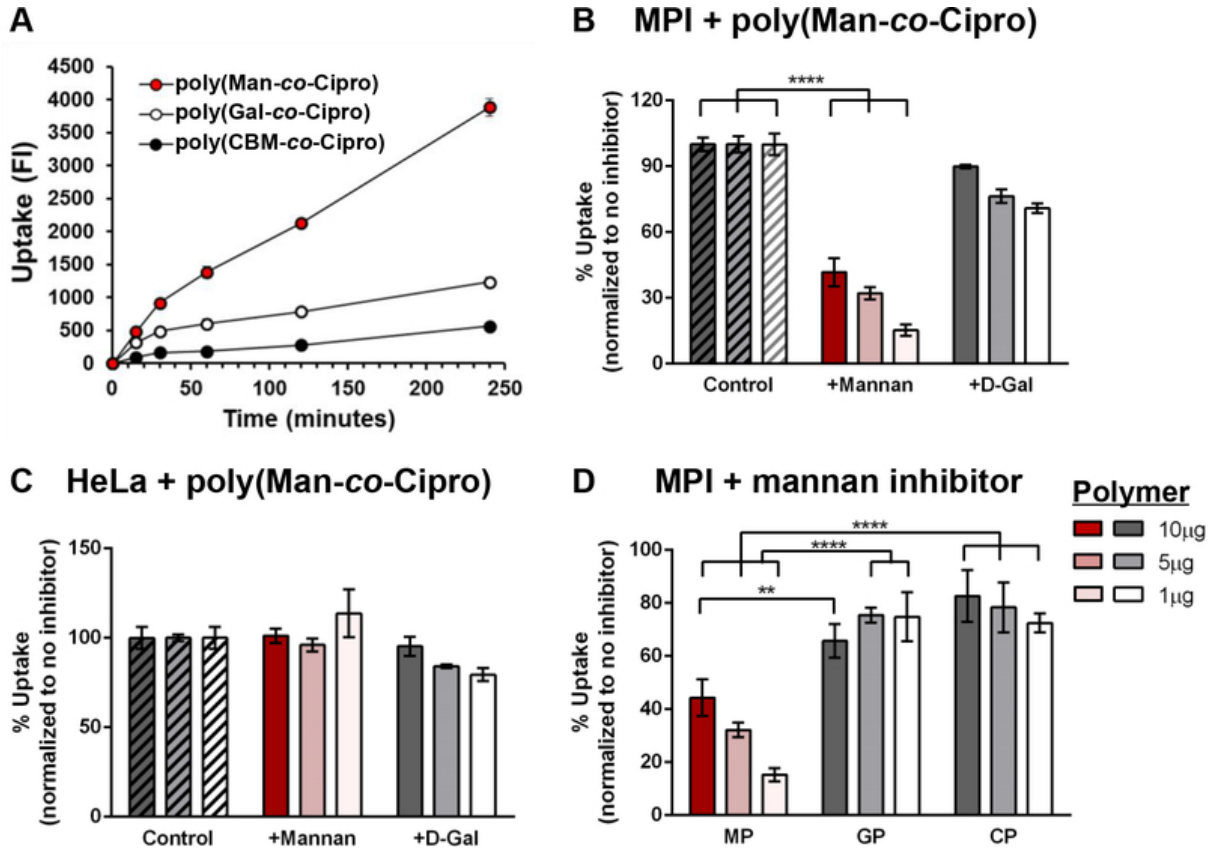

To evaluate the targeting capability *in vivo,* 3 mice each were dosed with a variant of the ciprofloxacin drugamers, incorporating a rhodamine labeled monomers (Figure 4). The incorporation of the rhodamine monomer, another example of the flexible modular nature of RAFT polymerization in drugamer synthesis discussed in section 1.2.1, confers fluorescence to the drugamers and enables quantification of drugamer uptake through fluorescence cytometry. Levels of rhodamine measured in alveolar macrophages treated with the fluorescent Man-drugamer were significantly higher than levels in either control drugamers, suggesting increased uptake of the Man-drugamer over either control drugamer (Figure 4b). Furthermore, significantly more cells contained rhodamine in the Man-drugamer treated mice than in the control treated mice (Figure 4b). This indicates that alveolar macrophages have a significant preference for Man-drugamer over the control drugamers (Figure 4b). Of the cells positive for fluorescence and containing drugamer, the cells from mice treated with Man-polymer expressed more fluorescence and internalized significantly more drugamer (Figure 4c). These results reinforce the findings in the *in vitro* experiments and confirm the targeting capability of the ciprofloxacin drugamer[16].

Figure 4. In vivo delivery of poly(Man-co-Cipro) to alveolar macrophages.

Rhodamine labeled Man-drugmaer (MP), Gal-drugamer (GP), and CBM-drugamer (CP) were administered to C57bl/6 mice. **(A)** Uptake of fluorescent drugamer compared to non-specific drugamer. **(B)** Comparison of the percentage of cells containing fluorescently labeled drugamer between each polymer prodrug treatment group. **(C)** Level of drugamer uptake (indicated by levels of fluorescence detection). The uptake of Man-drugamer was 2.4 times greater than that of control Gal-drugamer uptake, and 4.1 times greater than uptake of control CBM-polymer). [16]

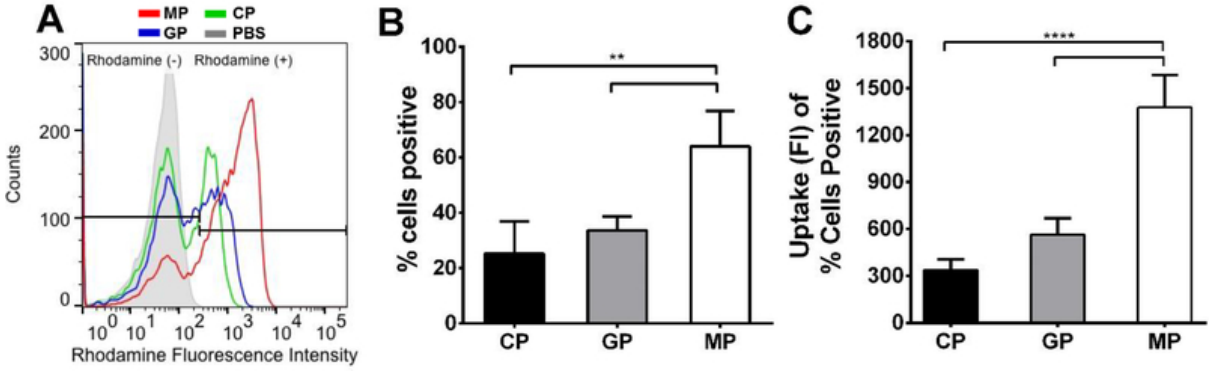

To ensure release of the drug only after internalization by the alveolar macrophages, two variants of the mannose targeted ciprofloxacin drugamers were synthesized with different linkers, a protease cleavable dipeptide (Man-co-VC) or a hydrolytic ester (Man-co-CTM). The VC linker, cleavable by the was theorized to allow cleavage and drug release only after internalization into the cellular lysosome by the human lysosomal protease cathepsin B (CatB). To verify linker accessibility and enzymatic cleavage, Man-co-VC was incubated with CatB (Figure 5). In the presence of CatB, Man-co-VC showed a half life of ~30 minutes, with no release observed from hydrolytic ester bearing Man-co-CTM during the experiment (Figure 5a,5b). To ensure that ciprofloxacin was released from Man-co-VC only through enzymatic cleavage after internalization within the lysosome, the drugamer was incubated under various aqueous conditions, including human serum, a buffer mimicking lysosomal pH, and CatB at neutral pH, stimulating CatB secreted outside the cell or expressed on the

cell membrane. Linker cleavage and ciprofloxacin release was only observed when incubated with CatB at lysosomal pH, with some release at neutral pH modeling the extracellular space, and no release from other conditions, indicating that drug release from the drugamer could only happen after endocytosis (Fig 5c). To examine if the ester bond in both linkers could be cleaved through non-specific esterase cleavage, both drugamers were incubated with the human esterase butrylcholinesterase, responsible for metabolizing ester-containing drugs and detoxification (Fig 5d). Although some non-specific esterase cleavage occurred, in comparison to the hydrolytic ester linked Man-co-CTM, Man-co-VC released significantly less ciprofloxacin (2.7% compared to 15.1% after 14 days), suggesting minimal drug release by non-specific esterase cleavage. In combination with the mannose targeting monomer, the use of the VC linker ensured that the polymer would be preferentially uptake by the alveolar macrophages and the drug released only after being internalized, achieving drug delivery to the intracellular space where the targeted pathogens *Burkholderia* and *Franciscella* reside[17].

Figure 5. Lysosomal protease-mediated drug release from polymeric ciprofloxacin prodrug.

(A) Release kinetics of ciprofloxacin from Man-co-VC or Man-co-CTM when incubated with CatB. (B) Ciprofloxacin release from Man-co-VC over time when incubated with CatB. (C) Release kinetics of ciprofloxacin during Man-co-VC with CatB (pH 5.0 or 7.4),, in human serum or in acetate buffer (pH 5.0). (D) Ciprofloxacin release from Man-co-VC when incubated a model esterase, human butyrylcholinesterase.[17]

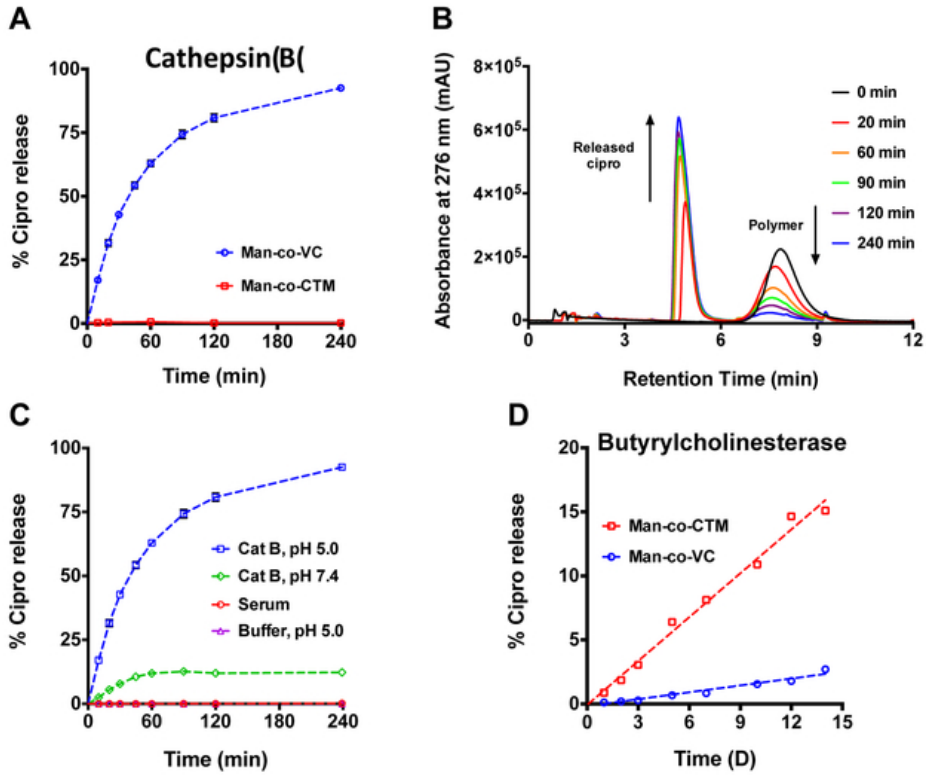

1.2.3 Controlled Release[18]

Drug release can be controlled by modification of drugamer structure and composition. More directly, the pro-drug monomer can be modified through selection of the linker between the pro-drug moiety and the drug. Incorporation of the dipeptide linker in Man-co-VC was theorized to prolong ciprofloxacin release. During incubation with macrophages, the Man-co-VC showed time-dependent release, with significantly more ciprofloxacin released than the

Man-co-CTM by hour 4 (Figure 6a)[17]. *In vivo,* we showed that ciprofloxacin had significantly higher and prolonged release with Man-co-VC than Man-co-CTM (Figure 7)[18] .

Figure 6. *In vitro* release, efficacy, and toxicity of polymeric ciprofloxacin prodrugs.

Released ciprofloxacin inside macrophages incubated Man-co-VC or Man-co-CTM.

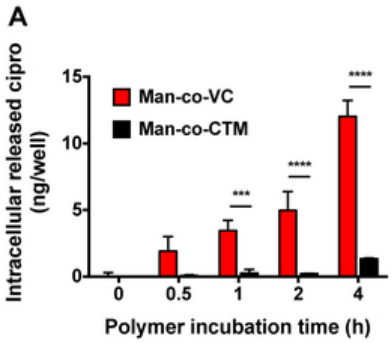

Fig. 7. *In vivo* pharmacokinetics of drugamer-released ciprofloxacin in alveolar macrophages.

Released ciprofloxacin 4 hours (day 0) to 7 days after dosing. Day 0 was defined as 4h after the drugamer administration. The lines indicate the average of the 3–4 data points of each time point. (n = 3–4)[18]

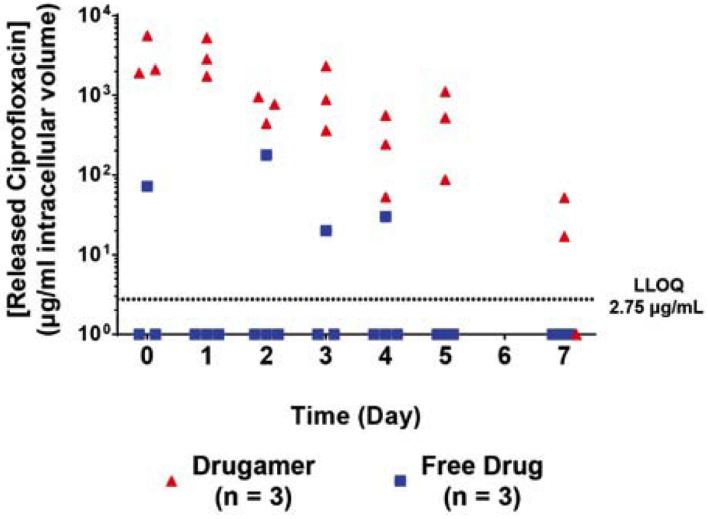

1.2.4 Efficacy

By combining monomers with varying components, multifunctional drugamers can be synthesized. This new inhalable "drugamer" therapeutic, Man-co-VC, is designed to achieve high and greatly extended dosing in the lung. This drugamer platform is shown to re-potentiate ciprofloxacin and to achieve full prophylaxis where the parent drug is ineffective against the antibiotic-resistant, Tier 1 select agent *Burkholderia pseudomallei*. This pulmonary drug platform builds delivery properties such as targeting and PK extension into the drug itself, rather than utilizing liposomal[21–23] or other nanoparticle[24,25,]formulations. This new therapeutic platform is a fully synthetic and modular version of past polymer therapeutics[26–28] .

This platform serves as a strikingly efficacious prophylactic in an aerosolized model of antibiotic-resistant *B. pseudomallei*. *B. pseudomallei* causes an estimated 165,000 cases of melioidosis per year, 89,000 annual deaths, and has a mortality rate of up to 50% in rural Thailand and Vietnam [29,30]. A major reason for the high mortality rate is that *B. pseudomallei* achieves protection from antibiotic exposure and adaptive immune responses through sequestration within the alveolar macrophage[31].

Current standard of care treatments rely on exhaustive antibiotic dosing regimens unchanged in decades[32]. Recommended treatments include 10–14 days or longer of intravenous therapy, followed by further 3-6 months of multi-daily oral antibiotic eradication therapy [29,32]. This lengthy and intensive treatment course is unavailable to many poor rural farmers, is associated with patient nonadherence, leads to well-documented patient side-effects, and

promotes the emergence of antibiotic-resistant bacteria[33]. While prophylactic use of antibiotics can be problematic in the context of drug resistance, the select and targeted use of prophylactic antibiotics has been advocated for in settings where health impacts are severe[34,35]. Given the small pipeline of new antibiotics, repurposing and re-potentiating existing antibiotics is therefore an important goal for pulmonary infections and *B. pseudomallei* in particular. This may be especially true for this current work that demonstrates repotentiation of the antibiotic ciprofloxacin to which *B. pseudomallei* is resistant clinically[36].

This drugamer platform targets the lung macrophage compartment as a reservoir to increase dosing against intracellular lung pathogens, as well as to extend drug PK out to seven days from a single dose (**Fig. 8**).The inhaled ciprofloxacin drugamer achieved 100% survival for the two-week study period, where the corresponding inhaled ciprofloxacin groups showed no efficacy and uniformly reached euthanasia endpoints after just 3 days. The modular drugamer platform is fully synthetic and thus manufacturing-ready with combination drug potential that can be exploited for response to other existing or emergent pulmonary infections[17,37–39].

Figure 8. Macrophage-targeted drugamer enables a sustained delivery of ciprofloxacin to alveolar macrophages.

Schematic showing the composition polymeric ciprofloxacin prodrug and its mechanism for enhancing alveolar macrophage uptake and intracellular antibiotic release. (1) The drugamer is composed of multivalent mannose ligands that act both as solubilizing agents and targeting residues, thus enhancing drugamer internalization by alveolar macrophages. (2) Drugamer binding to mannose receptors induces receptor-mediated endocytosis. The protease-cleavable dipeptide motif (Valine-Citrulline) linking ciprofloxacin to the polymer backbone is subsequently cleaved by intracellular proteases, such as cathepsins, allowing release of the antibiotic in the alveolar macrophage and killing of intracellular bacteria.

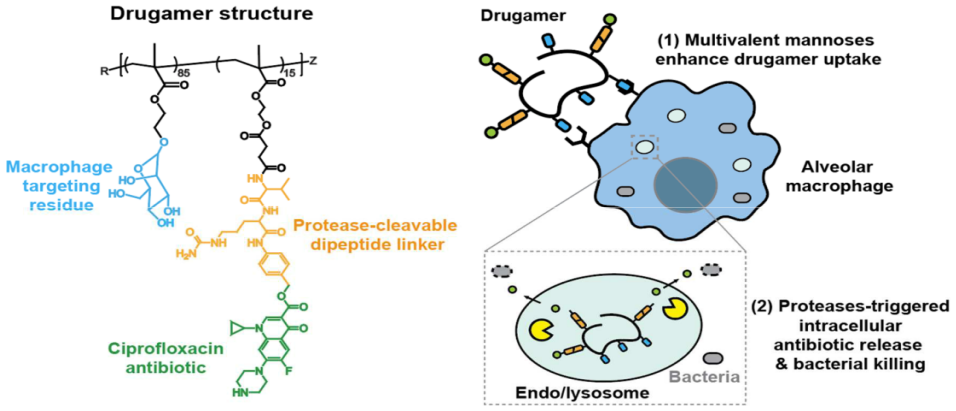

Table 1. Overall comparison of the three challenge studies reported. (MIC: Minimum inhibitory concentration)

	Figure 2	Figure 4	Figure 5
Bacterial strain	*B. thailandensis* E264 (Laboratory surrogate)	*B. thailandensis* E264 (Laboratory surrogate)	*B. pseudomallei* 1026b (Clinical isolate)
MIC_{50}/MIC_{90} (μg/mL)	2/4		2/2
Deposition dose* (CFU/Lung)	4.53×10^5	6.25×10^4	3.80×10^3
Dosing regimen†	Day 0, 1, 2	Day -2, -1, 0	Day -2, -1, 0
Suvival rate of drugamer treated mice	100% (8/8)	100% (8/8)	100% (10/10)
Suvival rate of free ciprofloxacin treated mice	25% (2/8)	12.5% (1/8)	0% (0/10)

*Bacterial deposition in the lungs was determined from quantitative culture of lung tissue from mice sacrificed immediately after infection (n=4).
†Bacterial infection was conducted at 2 h after the dosing on day 0.

The activity of the mannose-targeted, polymeric prodrug was initially evaluated in a murine model of pulmonary melioidosis brought about by exposure to *B. thailandensis* (**Table 1, Fig. 9**). This model is highly lethal in mice but not humans. Treatment with free ciprofloxacin provided a modest improvement in survival rates, with 25% (n = 2/8) of the mice remaining at the endpoint of 14 days. Administration of the polymeric ciprofloxacin prodrug led to full protection, with all mice surviving to 14 days (n = 8/8) (**Fig. 9A**). Though both free drug and drugamer-treated mice exhibited weight loss as soon as 24h post-infection, the latter had regained their baseline weight 5 days after the infection, compared with 9 days for the survivors of the former group. Of note, mice treated with free ciprofloxacin became visibly ill (e.g. decreased body temperature and increased morbidity) approximately 24h after infection, whereas these metrics remained stable for the drugamer-treated mice throughout the experiment (**Fig. 9B-D**). 14 days after infection, drugamer-treated mice (and the 2 survivors from the free ciprofloxacin-treated group) showed no detectable levels of bacteria in the lungs, spleen and liver (**Fig. 9E**), three organs that are commonly affected by melioidosis[40]. This is a strong indication that these mice had resolved the infection.

A comparative PK study of the drugamer and free ciprofloxacin was performed in mice (**Fig. 10**). The animals received a single intratracheal dose of 20 mg/kg ciprofloxacin – either in drugamer or free drug form – and were subsequently euthanized at pre-determined timepoints (4 hours – 7 days). The lung macrophages of the euthanized mice were collected through bronchoalveolar lavage, and liquid chromatography tandem mass spectrometry (LC-MS/MS) was used to measure the levels of ciprofloxacin in those cells. Inhaled ciprofloxacin was rapidly cleared as previously characterized[16,17,41] and after 4h, 33% of mice had

quantifiable levels of the drug in the alveolar macrophages. This is in stark contrast with what was observed for the drugamer. The concentration of ciprofloxacin observed in the alveolar

Fig. 9. Efficacy of the ciprofloxacin drugamer against aerosolized Burkholderia thailandensis E264.

Free ciprofloxacin (free drug) or ciprofloxacin drugamer were intratracheally administered (50 µL aerosolization, 20mg ciprofloxacin/kg) at day 0 (2h prior to the infection), 1, and 2 using a MicroSprayer® (n = 8 for each treatment group). PBS was used as a vehicle control. All mice were challenged with aerosolized *B. thailandensis* 2h after dosing on day 0. Survival rate and health condition of mice were monitored for 14 days. (A) Survival rate of infected mice. Arrows indicate dosing day. (B & C) Body weight and surface temperature of mice over the course of the experiment. (D) Clinical scores of mice. Mice were scored on seven categories: activity, coat, eyes, breathing, posture, isolation, and resistance to handling, with scores of 0, 0.5, and 1 specified for each category. E Bacterial burden in organs retrieved from mice that survived to the experimental endpoint (14 days). CFU: Colony-forming unit. Data are presented as mean ± SD. ** denotes $p < 0.01$.

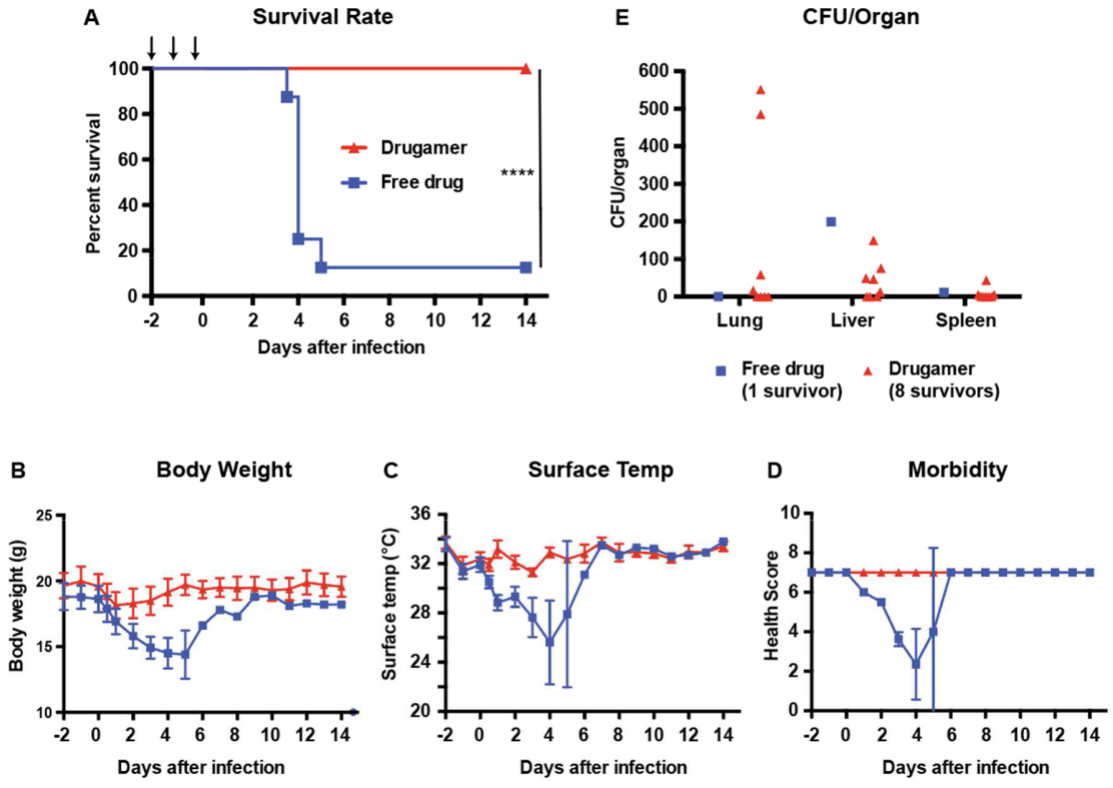

macrophage compartment was one to three orders of magnitude larger than that observed in mice dosed with the free drug, across all timepoints. All animals dosed with the drugamer also displayed detectable levels of ciprofloxacin in the alveolar macrophage compartment up to 5 days after administration, and two out of three mice exhibited detectable levels of ciprofloxacin in the alveolar macrophage compartment after 7 days.

The MIC of ciprofloxacin against *B. thailandensis* and *B. pseudomallei* are 2 and 4 μg/mL, respectively (**Table 2**). All the mice dosed with the drugamer had a ciprofloxacin concentration in the lungs that was above the MIC through the 7-day experiment, save for one mouse at the 7-day timepoint. Together, these observations demonstrate that the drugamer enables a delivery of ciprofloxacin to the alveolar macrophage compartment that was sustained over 5 to 7 days, with its concentration remaining orders of magnitude higher than when ciprofloxacin is administered as the free drug. Combined with the results from our successful challenge study with *B. thailandensis*, these observations prompted us to evaluate the efficacy of the drugamer in a fully prophylactic dosing regime

To test whether the polymeric prodrug was efficacious in a fully prophylactic dosing regimen, mice were dosed with the drugamer before being infected with *B. thailandensis* (**Fig. 10A**). The control group consisted of mice treated with an equivalent dose of free ciprofloxacin at the same time points. Apart from a modest and temporary decrease in body weight that was concurrent with the infection, the drugamer-treated group remained largely unaffected by the challenge with 100% survival (n = 8/8) at 14 days (**Fig. 10B-D**). This is in clear contrast with the 12.5% survival rate that resulted from treatment with free ciprofloxacin (1/8 survivors). A very significant drop in body weight, surface temperature

and health score was observed for all mice, from which 7/8 did not recover. The bacterial burden in the survivors was significantly reduced from the lethal inoculum (~ 10^5 CFU/lung) to sub-lethal levels (**Fig. 10E**).

Figure 10. Efficacy of the drugamer against a pulmonary *Burkholderia thailandensis* E264 infection in a pre-exposure prophylactic setting.

Free ciprofloxacin (free drug) or drugamer were intratracheally administered (50 µL aerosolization, 20mg ciprofloxacin/kg) at day -2, -1, and 0 using a MicroSprayer® (n = 8 for each treatment group). All mice were challenged with aerosolized *B. thailandensis* 2h after dosing on day 0. Survival rate and health condition of mice were monitored for 14 days. **(A)** Survival rate of infected mice. Arrows indicate dosing day. **(B & C)** Body weight and surface temperature of mice over the course of the experiment. **(D)** Clinical scores of mice. **(E)** Bacterial burden in organs retrieved from mice that survived to the experimental endpoint (14 days). Mice were scored on seven categories: activity, coat, eyes, breathing, posture, isolation, and resistance to handling, with scores of 0, 0.5, and 1 specified for each category. CFU: Colony-forming unit. Data are presented as mean ± SD.

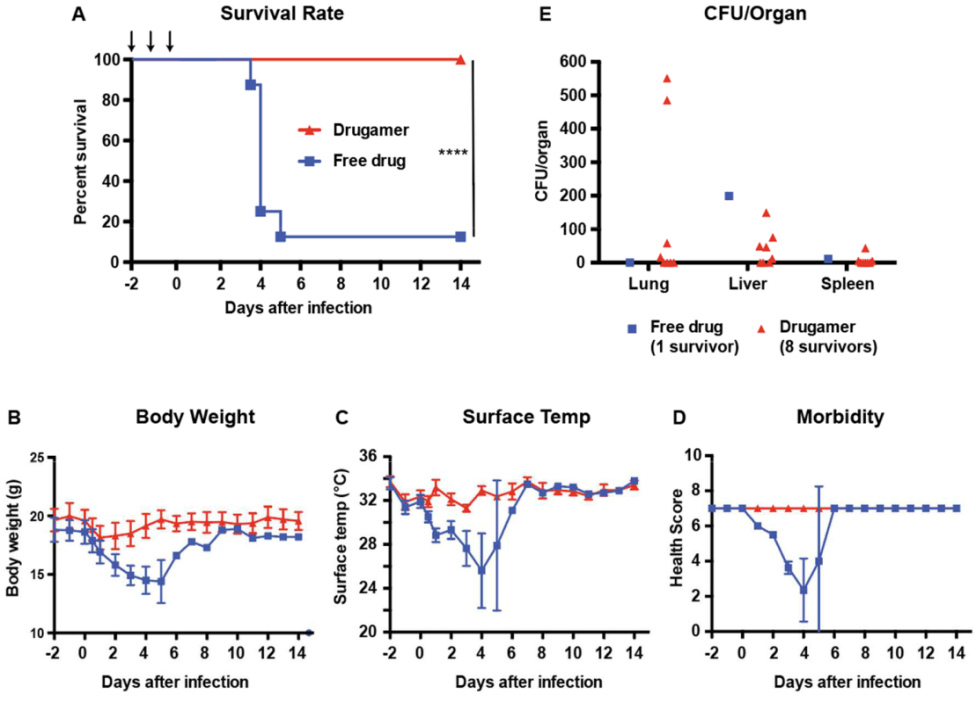

Having optimized our prophylactic treatment regimen against the surrogate strain, we characterized its efficacy in a virulent human-specific pathogen, *B. pseudomallei* 1026b [40]. Under conditions similar to our prophylactic challenge study against *B. thailandensis*, mice were dosed with the drugamer at 48h, 24h and 2h before being infected with *B. pseudomallei* (**Fig. 11A**). Control groups received an equivalent dose of the free drug (ciprofloxacin), or vehicle-treatment (PBS). The lethality of *B. pseudomallei* 1026b was apparent from the morbidity parameters: the surface temperature of vehicle-treated mice dropped below 25°C within two days of the infection, with a concomitant decrease in health score. As a result, all untreated mice had reached euthanasia criteria by day 4 (n = 10/10) as shown in **Fig. 11A**. With respect to body weight, temperature, morbidity scale, and survival rates, mice treated with free ciprofloxacin did not fare any better than vehicle-treated mice (**Fig. 11B-D**).

Figure 11. Pre-exposure prophylaxis efficacy of ciprofloxacin drugamer against a clinical isolate of *Burkholderia pseudomallei*.

PBS, free ciprofloxacin (free drug) or drugamer were intratracheally administered at day -2, -1, and 0 using a MicroSprayer® (n = 10 for each treatment group). PBS was used as a carrier control. All mice were challenged with aerosolized *B. pseudomallei* 2h after dosing on day 0. Survival rate and health condition of mice were monitored for 14 days. (A) Survival rate of infected mice. Arrows indicate dosing day. (B & C) Body weight and surface temperature of mice over the course of the experiment. (D) Clinical scores of mice. Mice were scored on seven categories: activity, coat, eyes, breathing, posture, isolation, and resistance to handling, with scores of 0, 0.5, and 1 specified for each category. (E) Bacterial burden in organs retrieved from mice that survived to the experimental endpoint (14 days). CFU: Colony-forming unit.

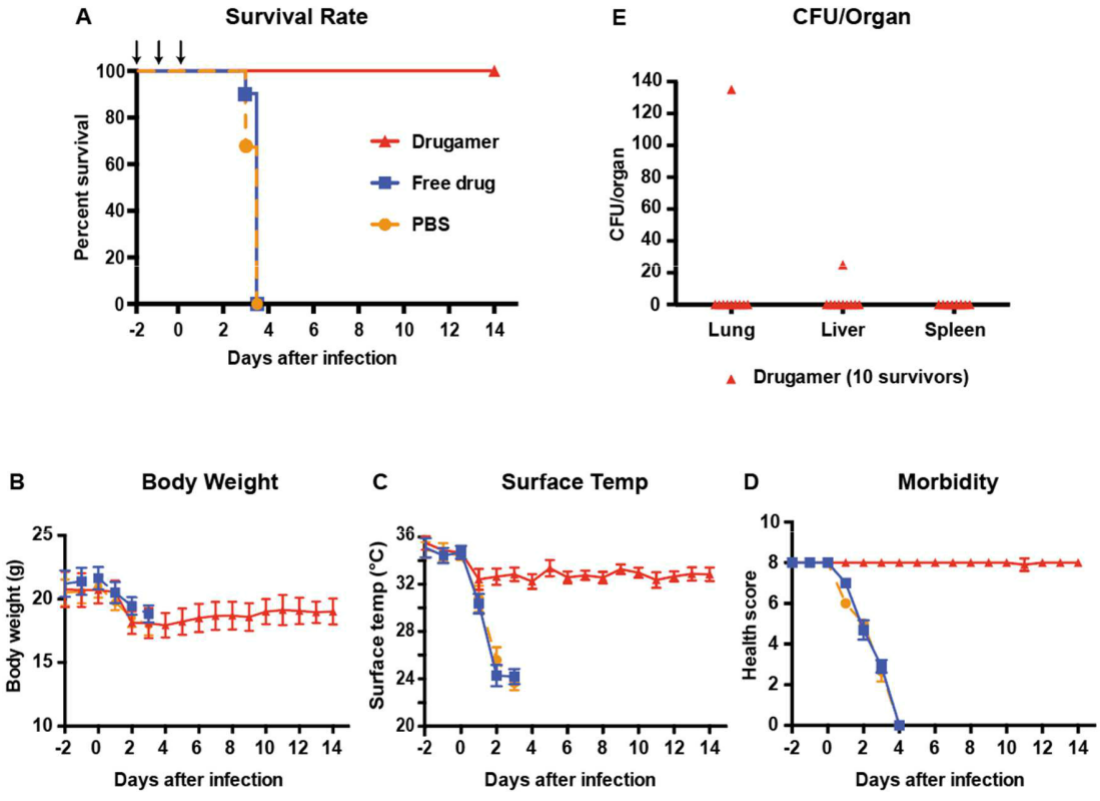

Through the drugamer platform, we successfully re-potentiated ciprofloxacin, mechanistically alter the drug's PK to dramatically lengthen intracellular dosing and target it more effectively to key bacterial reservoirs and sites of pathogenesis, the alveolar macrophage compartment. Contrasting with liposome-based formulations that rely on the

physical encapsulation of antibiotics and passive targeting to control PK, our drugamer exploits a cleavable peptide linker coupled with active macrophage-targeting ligands to achieve significantly better PK properties (sustained over 5-7 days) and striking therapeutic efficacy (full survival with merely 3 doses)

Ciprofloxacin is not considered a lead antibiotic for treating melioidosis due to its poor intrinsic treatment efficacy when freely administered[36,42,43]. Where free ciprofloxacin completely failed to protect the mice from *B. pseudomallei* (0% survival rates), our drugamer therapeutic offered full protection until the experimental endpoint of 14 days, by which 80% of the drugamer-treated group had completely cleared the pathogen (n = 8/10). This is a particularly significant result, given the relatively low intensity and duration of the regimen – a total of three doses of 20 mg/kg ciprofloxacin equivalent, spread over three days – when compared with the current standard of care in humans (2-3 doses/day for more than 3 months)[29,32].

As a reference point, reports characterizing the ciprofloxacin treatment of melioidosis in murine models have typically used more intensive regimens of ciprofloxacin: Barnes et al. dosed mice infected with *B. pseudomallei* K96243 with two daily doses of 30 mg/kg ciprofloxacin for 14 days[44], whilst Steward et al. treated mice infected with *B. pseudomallei* 576 with two daily doses of 100 mg/kg ciprofloxacin for 14 days[45]. Both studies reported high but not 100% survival in their treatment groups at 14 days after infection (90% and 95%, respectively), despite these lengthy and high intensity dosing regimens. The high activity of the drugamer therapeutics may enable the development of dose-sparing regimens by reducing duration and/or dose. Such properties would potentially avoid the emergence of

antibiotic resistance facilitated by the current standard of care for melioidosis, which involves intensive antibiotic treatment (multiple daily doses for 3-6 months)[29,32]. Moreover, the dose-sparing regimens that may be enabled by drugamers would be important to increase patient compliance, particularly in low-resource settings (e.g., rural Southeast Asia).

The improved efficacy of our drugamer can be attributed to its ability to modulate the biodistribution and PK properties of the antibiotic in the lungs and alveolar macrophages[17]. As observed in our PK studies, a single dose of the drugamer enables a delivery of ciprofloxacin to the alveolar macrophage compartment that is sustained over 5 days for all mice, and up to 7 days for two of the three mice sampled at that timepoint. Ciprofloxacin use for the treatment of melioidosis is ill-advised, both in humans[36,42,43] and in murine models[44,45] . This suggests that delivery of this antibiotic to the right target compartment and its short half-life are key factors limiting its efficacy. Repotentiating antibiotics through the use of this modular platform could provide a rationale for selected prophylactic use for global health since B. *pseudomallei* is resistant to fluoroquinolones. The number of doses and the dosing regimen for the future clinical development will need to be carefully decided based on the pharmacokinetic properties of antibiotics released from drugamers to avoid toxicities and minimize antibiotic usage.

The modularity of the drug repertoire has been shown with other prodrug monomers[37–39], and could thus be expanded to other pulmonary infection space, including other antibiotics, antivirals and host-directed drugs. The fully synthetic platform has intrinsic scalability, streamlined CMC, and an on-demand, rapid response potential using existing GMP manufacturing infrastructure. These features make the platform a promising candidate for

pulmonary infection therapy against intransient existing pathogens and current and future emergent pandemic threats.

1.3 Overall Objective

In this thesis, I demonstrate how the RAFT drugamer platfomr can be used to modify properties such as administration method, pharmacokinetics, and targeting through two different projects: development of a nano-fiber based tenofivir drugamer and evaluation of the Man-co-VC polymer targeting a different pulmonary infection setting, biofilms.

1.3.1 Nano-fiber based anti-viral Tenofivir prodrug delivery system

Hepatitis B and HIV are two of the most prevalent infections, both necessitating complex daily medications. While some progress has been made in the development of long-acting medications with the development of some long acting medications, there is still a need for more advanced and longer-lasting delivery vehicles with different modes of application to increase access to medication for patients with viral infections Using the drugamer platform, we aimed to synthesize a drugamer bearing tenofovir alafenamide (TAF) for fabrication into nanofibers to create an extended release antiviral pro-drug with a different mode of application.

1.3.2 Glycan targeted pro-drug system

Glycans, with their wide structural diversity and microheterogeneity, are known to play a variety of major biological roles, including signaling, mediating cellular interactions, and

modulating activity. Experiments with Pseudomonas have identified specific mannose-binding proteins within the pseudomonas biofilm that can be exploited to deliver therapeutics to the biofilm with the same drugamer platform. As key constituents of the *Pseudomonas* biofilm, CdrA and Lec B, are known to bind strongly to Psl, a polysaccharide composed of mannose, a mannosylated drugamer could be bound to and integrated into the *Pseudomonas* biofilm for extended antibiotic retention. We aimed to evaluate targeting and pharmacokinetics of Man-co-VC to *Pseudomonas aeruginosa* biofilm, showing how the Man-co-VC polymer could be applied to different disease settings.

References

Figures and text from sections 1.2.3 and 1.2.4 are originally published in Chavas, T. E. J. *et al.* A macrophage-targeted platform for extending drug dosing with polymer prodrugs for pulmonary infection prophylaxis. *J. Controlled Release* **330**, 284–292 (2021).

1. Cahaya, N., Kristina, S. A., Widayanti, A. W. & Green, J. Interventions to Improve Medication Adherence in People with Schizophrenia: A Systematic Review. *Patient Prefer. Adherence* **16**, 2431–2449 (2022).

2. Kaplan, G., Casoy, J. & Zummo, J. Impact of long-acting injectable antipsychotics on medication adherence and clinical, functional, and economic outcomes of schizophrenia. *Patient Prefer. Adherence* **7**, 1171–1180 (2013).

3. Correll, C. U. *et al.* Three-Year Outcomes of 6-Month Paliperidone Palmitate in Adults With Schizophrenia: An Open-Label Extension Study of a Randomized Clinical Trial. *JAMA Netw. Open* **7**, e2421495 (2024).

4. Considine, E. G. & Sherr, J. L. Real-World Evidence of Automated Insulin Delivery System Use. *Diabetes Technol. Ther.* **26**, 53–65 (2024).

5. Sherr, J. L. *et al.* Automated insulin delivery: benefits, challenges, and recommendations. A Consensus Report of the Joint Diabetes Technology Working Group of the European Association for the Study of Diabetes and the American Diabetes Association. *Diabetologia* **66**, 3–22 (2023).

6. Steenkamp, D., Eby, E. L., Gulati, N. & Liao, B. Adherence and Persistence to Insulin Therapy in People with Diabetes: Impact of Connected Insulin Pen Delivery Ecosystem. *J. Diabetes Sci. Technol.* **16**, 995–1002 (2021).

7. Edwards, G. G. *et al.* Long-Acting Injectable Therapy for People with HIV: Looking Ahead with Lessons from Psychiatry and Addiction Medicine. *AIDS Behav.* **27**, 10–24 (2023).

8. Foster, J. M. *et al.* Higher patient perceived side effects related to higher daily doses of inhaled corticosteroids in the community: a cross-sectional analysis. *Respir. Med.* **100**, 1318–1336 (2006).

9. Coleman, N. & Rodon, J. Taking Aim at the Undruggable. *Am. Soc. Clin. Oncol. Educ. Book Am. Soc. Clin. Oncol. Annu. Meet.* **41**, 1–8 (2021).

10. Zhou, Z. & Li, M. Targeted therapies for cancer. *BMC Med.* **20**, 90 (2022).

11. Hoang, T., Myung, S.-K., Pham, T. T., Kim, J. & Ju, W. Comparative Efficacy of Targeted Therapies in Patients with Non-Small Cell Lung Cancer: A Network Meta-Analysis of Clinical Trials. *J. Clin. Med.* **9**, 1063 (2020).

12. Li, P., Jahnke, J., Pettit, A. R., Wong, Y.-N. & Doshi, J. A. Comparative Survival Associated With Use of Targeted vs Nontargeted Therapy in Medicare Patients With Metastatic Renal Cell Carcinoma. *JAMA Netw. Open* **2**, e195806 (2019).

13. Rautio, J. *et al.* Prodrugs: design and clinical applications. *Nat. Rev. Drug Discov.* **7**, 255–270 (2008).

14. Chiefari, J. *et al.* Living Free-Radical Polymerization by Reversible Addition−Fragmentation Chain Transfer: The RAFT Process. *Macromolecules* **31**, 5559–5562 (1998).

15. McCormick, C. L. & Lowe, A. B. Aqueous RAFT Polymerization: Recent Developments in Synthesis of Functional Water-Soluble (Co)polymers with Controlled Structures. *Acc. Chem. Res.* **37**, 312–325 (2004).

16. Jasmin, C. *et al.* Glycan targeted polymeric antibiotic prodrugs for alveolar macrophage infections. *Biomaterials* **195**, 38–50 (2019).

17. Su, F.-Y. *et al.* Macrophage-targeted drugamers with enzyme-cleavable linkers deliver high intracellular drug dosing and sustained drug pharmacokinetics against alveolar pulmonary infections. *J. Controlled Release* **287**, 1–11 (2018).

18. Chavas, T. E. J. *et al.* A macrophage-targeted platform for extending drug dosing with polymer prodrugs for pulmonary infection prophylaxis. *J. Controlled Release* **330**, 284–292 (2021).

19. Limqueco, E. *et al.* Mannose Conjugated Polymer Targeting *P. aeruginosa* Biofilms. *ACS Infect. Dis.* **6**, 2866–2871 (2020).

20. Mitsi, E. *et al.* Human alveolar macrophages predominately express combined classical M1 and M2 surface markers in steady state. *Respir. Res.* **19**, 66 (2018).

21. Hamblin, K. A. *et al.* Inhaled Liposomal Ciprofloxacin Protects against a Lethal Infection in a Murine Model of Pneumonic Plague. *Front. Microbiol.* **8**, 91–91 (2017).

22. Norville, I. H. *et al.* Efficacy of liposome-encapsulated ciprofloxacin in a murine model of Q fever. *Antimicrob. Agents Chemother.* **58**, 5510–5518 (2014).

23. Hamblin, K. A. *et al.* Liposome encapsulation of ciprofloxacin improves protection against highly virulent Francisella tularensis strain Schu S4. *Antimicrob. Agents Chemother.* **58**, 3053–3059 (2014).

24. Moghimi, S. M., Hunter, A. C. & Andresen, T. L. Factors Controlling Nanoparticle Pharmacokinetics: An Integrated Analysis and Perspective. *Annu. Rev. Pharmacol. Toxicol.* **52**, 481–503 (2012).

25. Yamashita, F. & Hashida, M. Pharmacokinetic considerations for targeted drug delivery. *Adv. Drug Deliv. Rev.* **65**, 139–147 (2013).

26. DUNCAN, R. *et al.* Fate of N-(2-hydroxypropyl)methacrylamide copolymers with pendent galactosamine residues after intravenous administration to rats. *Biochim. Biophys. Acta BBA - Gen. Subj.* **880**, 62–71 (1986).

27. Ringsdorf, H. Structure and properties of pharmacologically active polymers. *J. Polym. Sci. Polym. Symp.* **51**, 135–153 (1975).

28. Kopeček, J. & Duncan, R. Targetable polymeric prodrugs. *J. Controlled Release* **6**, 315–327 (1987).

29. Currie, B. Melioidosis: Evolving Concepts in Epidemiology, Pathogenesis, and Treatment. *Semin. Respir. Crit. Care Med.* **36**, 111–125 (2015).

30. Limmathurotsakul, D. *et al.* Predicted global distribution of Burkholderia pseudomallei and burden of melioidosis. *Nat. Microbiol.* **1**, 15008 (2016).

31. Allwood, E. M., Devenish, R. J., Prescott, M., Adler, B. & Boyce, J. D. Strategies for Intracellular Survival of Burkholderia pseudomallei. *Front. Microbiol.* **2**, 170–170 (2011).

32. Dance, D. Treatment and prophylaxis of melioidosis. *Int. J. Antimicrob. Agents* **43**, 310–318 (2014).

33. Ventola, C. L. The antibiotic resistance crisis: part 1: causes and threats. *P T Peer-Rev. J. Formul. Manag.* **40**, 277–283 (2015).

34. Estes, D. M., Dow, S. W., Schweizer, H. P. & Torres, A. G. Present and future therapeutic strategies for melioidosis and glanders. *Expert Rev. Anti Infect. Ther.* **8**, 325–338 (2010).

35. MacLaren, G., Lye, D. C. & Lee, V. J. Increasing Experience With Melioidosis and Critical Care: Medical and Military Implications*. *Crit. Care Med.* **44**, 1608–1609 (2016).

36. Chaowagul, W., Suputtamongkul, Y., Smith, M. D. & White, N. J. Oral fluoroquinolones for maintenance treatment of melioidosis. *Trans. R. Soc. Trop. Med. Hyg.* **91**, 599–601 (1997).

37. Son, H. N. *et al.* Chemotherapeutic copolymers prepared via the RAFT polymerization of prodrug monomers. *Polym. Chem.* **7**, 4494–4505 (2016).

38. Kern, H. B. *et al.* Enzyme-Cleavable Polymeric Micelles for the Intracellular Delivery of Proapoptotic Peptides. *Mol. Pharm.* **14**, 1450–1459 (2017).

39. Freeman, H., Srinivasan, S., Das, D., Stayton, P. S. & Convertine, A. J. Fully synthetic macromolecular prodrug chemotherapeutics with EGFR targeting and controlled camptothecin release kinetics. *Polym. Chem.* **9**, 5224–5233 (2018).

40. Warawa, J. M. Evaluation of surrogate animal models of melioidosis. *Front. Microbiol.* **1**, 141–141 (2010).

41. Cipolla, D., Blanchard, J. & Gonda, I. Development of Liposomal Ciprofloxacin to Treat Lung Infections. *Pharmaceutics* **8**, 6 (2016).

42. Ashdown, L. R. & Currie, B. J. Melioidosis: when in doubt leave the quinolone alone! *Med. J. Aust.* **157**, 427–428 (1992).

43. Chetchotisakd, P., Chaowagul, W., Mootsikapun, P., Budhsarawong, D. & Thinkamrop, B. Maintenance therapy of melioidosis with ciprofloxacin plus azithromycin compared with cotrimoxazole plus doxycycline. *Am. J. Trop. Med. Hyg.* **64**, 24–27 (2001).

44. Barnes, K. B. *et al.* Demonstrating the Protective Efficacy of the Novel Fluoroquinolone Finafloxacin against an Inhalational Exposure to Burkholderia pseudomallei. *Antimicrob. Agents Chemother.* **61**, e00082-17 (2017).

45. Steward, J. *et al.* Comparison of gatifloxacin, moxifloxacin and ciprofloxacin for treatment of experimental Burkholderia pseudomallei infection. *J. Antimicrob. Chemother.* **55**, 523–527 (2005).

46. Dart, A. *et al.* A nanofiber based antiviral (TAF) prodrug delivery system. *Biomater. Adv.* **133**, 112626 (2022).

2 Nano-fiber based anti-viral Tenofivir prodrug delivery system

2.1 Abstract

HIV and hepatitis B are two of the most prevalent viruses globally, and despite readily available preventive treatments unforgiving treatment regimens still exist, such as daily doses of medicine that are challenging to maintain especially in poorer countries. More advanced and longer-lasting delivery vehicles can potentially overcome this problem by reducing maintenance requirements and significantly increase access to medicine. Here, we designed a technology to control the delivery of an antiviral drug over a long timeframe via a nanofiber based delivery scaffold that is both easy to produce and use. An antiviral prodrug containing tenofovir alafenamide (TAF) was synthesized by initial conjugation to glycerol monomethacrylate followed by polymerization to form a diblock copolymer (pTAF) using reversible addition-fragmentation chain transfer (RAFT). In order to generate an efficient drug delivery system this copolymer was fabricated into an electrospun nanofiber (ESF) scaffold using blend electrospinning with poly(caprolactone) (PCL) as the carrier polymer. SEM images revealed that the pTAF-PCL ESFs were uniform with an average diameter of (787 ± 0.212 nm), while XPS analysis demonstrated that the pTAF was overrepresented at the surface of the ESFs. Additionally, the pTAF exhibited a sustained release profile over a 2 month period in human serum (HS), suggesting that these types of copolymer-based drugamers can be used in conjunction with electrospinning to produce long-lasting drug delivery systems.

2.2 Literature Review

Hepatitis B and HIV are two of the most prevalent viruses globally [1], [2]. Developed markets with adequate access to antiviral treatments have severely reduced the morbidity and impact of these viruses, however, these programs and technologies lie out of reach for people in resource-limited countries [3]. HIV is a major medical challenge with approximately 37.9 million people infected worldwide [4]. Daily medicine is currently required to control the infection, which have various negative impacts on both mental and physical health [5], [6]. While there are prevention technologies available to limit the spread of the infection, these sources have only had limited effectiveness [2]. Hepatitis B also disproportionately affects the developing world, with 257 million people infected with the virus in 2017 [7]. Of these, however, only 27 million (10.5%) are actually aware of their infection, and from that pool, just 4.5 million people are able to receive regular treatment. Also, it is estimated that 15% to 40% of those infected will develop serious sequelae such as, cirrhosis or hepatocellular carcinoma. This leaves 34 to 98.3 million people potentially vulnerable to these sequelae [8]. It is clear that there are gaps that still need to be addressed in the effective treatment of the majority of those infected, whether it be health education, detection and treatment accessibility.

Tenofovir alafenamide (TAF) is a recently developed prodrug reverse transcriptase inhibitor used to prevent the spread of HIV, which is achieved by inhibition of the activity of HIV-1 reverse transcriptase by competing with the natural substance. Additionally, TAF is used in treatment of chronic hepatitis B, as it is also a competitive inhibitor of Hepatitis B virus

(HBV) polymerase [9], [10]. TAF is a prodrug of Tenofovir, and prodrugs have the advantage of being activated after metabolism in the target area of the body. This attribute reduces the severity of side effects of the drug, however, side effects are still widely reported [11]. In addition to these side effects, the relatively short half-life of these prodrugs results in preventive or treatment medications to be administered daily [11], [12], resulting in expensive and inaccessible treatment programs for patients outside developed markets [3].

New delivery vehicles have been developed to combat the short half-life of antivirals and further improve cell targeting to reduce side effects, such as combining drugs with nanoparticles, attachment of drugs to large proteins such as lactoferrin, or conjugation of prodrugs to hydrophilic polymers [13], [14], [15], [16], [17]. Drug targeting and half-lives have been shown to be improved by conjugating hydrophilic polymers to prodrugs using reversible addition-fragmentation chain-transfer (RAFT) polymerization [13]. This new class of pharmaceuticals is designed with enzyme-cleavable linkers that are targeted for intracellular activation, thus further limiting potential side effects from unintended activation elsewhere in the body, while also increasing the half-life of the drug substantially [13].

More advanced technologies can improve treatment accessibility to better cater for the disproportionally higher number of patients who have only limited access to adequate healthcare. Currently hepatitis B and HIV treatment is dependent on the regular ingestion of short half-life antiviral drugs such as tenofovir and entecavir [10], [12]. Producing a more efficient platform for distribution of active agents has the potential to improve treatment costs and accessibility, which are key factors in treating hepatitis B or HIV [18], [19].

Alternative delivery methods, such as injectable long-acting formulations, have been shown to be effective up to 8 weeks in clinical trials [20]. More advanced implantable delivery methods have shown the ability to deliver medicine up to 9 months experimentally, with the added benefit of removal of the drug delivery system if necessary [21]. TAF has also been shown to be able to be delivered via long acting subcutaneous implants [22]. Other delivery methods such as electrospun fiber (ESF) patches and hydrogels have also been explored for the delivery of various antiviral medicines, and patch style delivery methods have the added benefit of being noninvasive and easy to remove (Table 2) [18], [23], [24].

Antiviral drug	Delivery method	Stage of development	Reference
TAF	Oral (tablet)	Commercial	[12]
TAF	Oral (powder)	Commercial	[12]
Cabotegravir and rilpivirine	Injection	Clinical	[20]
Dolutegravir	Injection	Experimental	[21]
TAF	Subcutaneous implant	Experimental	[22]
Subtilosin	Electrospun fiber patch	Experimental	[18]
Griffithsin	Electrospun fiber patch	Experimental	[23]
Acyclovir	Hydrogel	Experimental	[24]

Table 2: Drug delivery methods for antiviral drugs currently in use.

Electrospinning has been identified as a new drug delivery technology as it allows for the production of micro to nanoscale fiber meshes that can be upscaled to commercial quantities [25]. Thus, electrospun patches incorporated with the next generation of drugs such as polymer-conjugated prodrugs and other developing technologies could produce an innovative system to treat and prevent infectious diseases [13], [25], [26]. Poly(caprolactone) (PCL) is a polymer ideal for drug delivery purposes since it has a long biodegradation time and is biocompatible, and when blended with hydrophilic polymers can form core-shell structures in resultant ESFs [27]. In addition, ESFs can be produced containing additives in which the additive and scaffold polymer are mixed in the same electrospinning solution prior to fiber generation. If the additive is evenly distributed throughout the fibers it can result in stable release over a longer timeframe [25], [28].

In this work we have designed a new antiviral strategy synthesized via RAFT polymerization. The polymer consists of a methacrylate-based TAF prodrug monomer with a *para*-hydroxybenzyloxycarbonyl (PHBC) spacer that is used to form a diblock copolymer containing glycerol monomethacrylate (pTAF) by using RAFT polymerization. The TAF di-block copolymer was incorporated into a PCL ESF scaffold via blend electrospinning. A sustained release of the TAF-diblock was observed from the fiber scaffold over a 2 month period, suggesting that this technology can potentially be developed to replace or complement current oral prescriptions or be used as an antiviral delivery patch with improved functionality.

2.3 Methodology

2.3.1 Materials

Chain-transfer agents, 4-(((2-carboxyethyl)thiocarbonothioyl)thio)-4-cyanopentanoic acid (CCC) were purchased from Boron Molecular (Texas, USA). Glycerol monomethacrylate was purchased from Polysciences and purified using basic alumina before polymerization. Recrystallized initiator, azobisisobutyronitrile (AIBN) was purchased from Sigma Chemicals (J. T. Baker, Phillipsburg, New Jersey, USA). Fasudil hydrochloride was purchased from eNovation Chemicals (Green Brook, NJ, USA). Spectra/Por regenerated cellulose dialysis membranes were purchased from Spectrum Laboratories (Houston, Texas, USA). Tenofovir alafenamide fumarate (TAF) was purchased from MedKoo Biosciences (Morrisville, North Carolina, USA). Analytical standards Tenofovir (TFV) and Tenofovir diphosphate (TFV-DP) were obtained from Cayman Chemicals (Ann Arbor, Michigan, USA and Santa Cruz Biotech, Dallas, Texas, USA), respectively. Tenofovir-d_6 (TFV-d_6) was purchased from Toronto Research Chemicals (Toronto, Ontario, Canada). HPLC grade methanol, acetonitrile and water were purchased from VWR International (Radnor, Pennsylvania, USA). Electrospinning chemicals such as poly(caprolactone) (PCL) (MW 80000) polymer and solvents dimethylformamide (DMF) (AR grade 99.9+% purity) and chloroform were acquired from Sigma-Aldrich Inc. (Castle Hill, New South Wales, Australia). Silicon wafers were purchased from M.M.R.C. Pt Ltd. (Malvern, Victoria, Australia).

2.3.2 Synthesis of TAF prodrug monomers

Synthetic steps outlined in Fig. 1 were followed to obtain TAF benzyl carbamate (***6***) monomer. All the synthesized compounds were purified by precipitation and/or silica gel column chromatography. The successful synthesis and purity of the monomers were confirmed and characterized by ^{1}H NMR spectroscopy (Bruker Avance spectrometers 300 MHz) and electrospray ionization mass spectrometry (Bruker Esquire ion trap mass spectrometer). The full synthetic procedures and associated characterization data are detailed in the supporting information.

2.3.3 Synthesis of macro chain transfer agent (pGMA) and TAF diblock copolymer

The full synthetic procedures and associated characterization data of macro CTA and TAF diblock copolymer are detailed in the supporting information.

2.3.4 Electrospinning solution formulation

Samples were prepared by first dissolving polymer powders of known weight in a mixed solvent of DMF/chloroform with a ratio of 2:3. Two samples were generated, a control PCL DMF/chloroform solution, and a blend pTAF-PCL solution containing 10% w v^{-1} of PCL and 2.5% w v^{-1} of pTAF (i.e. a w v^{-1} ratio of 4:1).

2.3.5 Electrospinning of PCL and PCL-pTAF ESFs

Electrospinning of polymer solutions was carried out on a custom-built apparatus described previously [29]. All electrospinning experiments were carried out at room temperature with a relative humidity of 40% to 60%. Solutions were loaded into a 5 mL syringe which was connected to an 18 gauge blunt needle that was positively charged. A grounded metal plate was used as the collector, and samples were collected on Al foil that covered the collector. Control PCL solution was electrospun with the following parameters: voltage of 11 kV and flowrate of 1.0 mL hr^{-1} with a deposition time of 60 min, which was found to produce consistent fibers. The PCL-pTAF solution had the electrospinning parameters adjusted due to the addition of pTAF, to a voltage of 13 kV and flowrate of 1.1 mL h^{-1} to produce a stable Taylor cone and optimize fiber formation (Table 3).

Table 3: Optimized electrospinning parameters for PCL pTAF blend polymer solutions.

Sample	Polymer %w	pTAF %w	Flow rate (mL h^{1})	Voltage (kV)	Deposition time (min)
PCL control	10%	0%	1	11	60
PCL-pTAF	10%	2%	1.1	13	60

2.3.6 Spin coating of pure pTAF samples

Samples of pTAF were dissolved in the electrospinning solvent and spin-coated onto silicon wafers to generate a thin film of pTAF that could be analyzed with XPS. 1 cm^2 Si wafers were cleaned via sonication in Decon 90 solution for 30 min, followed by 10 min in Milli Q water and a further 10 min in isopropyl alcohol (IPA) solution. Wafers were then rinsed with

IPA 3 times before being dried with compressed nitrogen. Spin-coating onto the cleaned wafers was achieved with a 2.5% w v^{-1} pTAF solution which is the same concentration used for electrospinning, using a P6700 spin coater at RPM of 600 for 100 s. Spin-coated samples were analyzed by XPS for comparison to PCL and PCL-pTAF ESFs.

2.3.7 Characterization of the fibers and polymer surfaces

Scanning electron microscopy (SEM) was used to determine the uniformity of the ESF meshes by visually assessing for any formation of beads and other defects, and to determine the average fiber diameter. Both PCL control and PCL-pTAF ESF samples were scanned in triplicate. Fiber meshes were coated with a 10 nm layer of conductive gold via sputter coating (K975X Turbo Evaporator) before SEM imaging, which was carried out with the FE-SEM ZEISS SUPRA 40 VP. Fibers were scanned with an accelerating voltage of 3KeV at a magnification of 5000×. Single fibers were measured at random from captured images using ImageJ software (Version 1.51 g) to determine average fiber diameter within each mesh.

Chemical analysis was carried out with X-ray photoelectron spectroscopy (XPS). Control PCL fibers, ESF-pTAF composite fibers and pTAF spin-coated surfaces were analyzed in triplicate. A Kratos Analytical Axis Nova was used with a monochromated aluminum X-ray source ($Al_{k\alpha}$, $h\nu$ = 1486.6 eV) operating at a power of 225 W (15 mA and 15 kV). Each sample was analyzed to acquire the following spectra: survey spectra between 0 and 1200 eV with a pass energy (PE) of 160 eV for elemental composition, and high-resolution C1s, N1s, and O1s all acquired with a PE of 20 eV for chemical state information. CasaXPS software version 2.3.18PR1.0 (Casa Software Ltd., Teignmouth, UK) was used for data analysis. All

spectra were calibrated using the C-C/C-H peak in the C 1s spectrum at 285.0 eV. Atomic concentrations of the identified elements were determined via integral peak intensities and sensitivity factors supplied by the manufacturer, with trace elements (<0.1 atom %) removed. Fiber composition was then compared to theoretical composition, literature sources and control samples where appropriate [30]. The high resolution spectra were curve-fitted with a Gaussian-broadened Lorentzian functions (G/L = 30) after linear background subtraction. A restriction of 1.2–1.6 eV full width half maximum (FWHM) was employed with the peaks generated. C1s spectral analysis was limited to the range between 282.0 and 292.0 eV, as no significant C1s peaks were detected beyond those binding energies. Multiple different carbon environments were resolved for each type of sample, of particular interest being the detection of new carbon environments with the addition pTAF. N1s spectral analysis was limited to between 388.0 and 406.0 eV, N1s curve-fitting being done in a similar way to C1s fitting, using the C-C/C-H calibrated peak from the C1s high resolution spectra. Peaks were again resolved and fitted as above, with the same FWHM restriction applied.

2.3.8 In vitro drug release of ESF pTAF and analysis by LC-MS/MS

ESF-pTAF (36.1 mg) fibers were removed from the foil backing and placed in 14.44 mL of human serum medium (HS) and incubated at 37 °C under constant agitation in an orbital shaker. After each incubation period, three separate 50 µL aliquots of HS were withdrawn and immediately stored at −80 °C until further processing. At each withdrawal, 150 µL Serum HS that was incubated at 37 °C in parallel was added to restore the medium volume. Sample processing details are described in the Supporting Information. Briefly, samples

spiked with internal standard TFV-d_6 were purified via a methanol precipitation prior to analysis via liquid chromatography-tandem mass spectrometry (LC-MS/MS) on a Waters Xevo TQ-S instrument. The linear gradient was as follows: 0–0.8 min, 0.25 mL min^{-1}, 5% B; 0.8–1 min, 0.25 mL min^{-1}, 15% B; 1–3.5 min, 0.25 mL min^{-1}, 20% B; 3.5–4.5 min, 0.25 mL min^{-1}, 20% B; 4.5–7.5 min, 0.25 mL min^{-1}, 60% B; 7.5–9 min, 0.25 mL min^{-1}, 74% B; 9–9.1 min, 0.25 mL min^{-1}, 85% B; 9.1–9.5 min, 0.25 mL min^{-1}, 90% B; 9.5–10 min, 0.30 mL min^{-1}, 90% B; 10–10.5 min, 0.3 mL min^{-1}, 90% B; 10.5–11.5 min, 0.3 mL min^{-1}, 5% B; 11.5–11.6 min, 0.3 mL min^{-1}, 5% B; 11.6–12 min, 0.25 mL min^{-1}, 5% B.

2.4 Results and Discussion

2.4.1 Synthesis and characterization of TAF prodrug monomer

We designed a methacrylate based TAF prodrug monomer carrying a para-hydroxybenzyloxycarbonyl (PHBC) spacer between the polymerizable unit and TAF, that can be directly polymerized by reversible addition fragmentation chain-transfer (RAFT) polymerization [31]. The PHBC spacer is well known for its self-immolative nature; once the phenolic ester bond is hydrolyzed, the resulting phenolate quickly self-eliminates and triggers the spontaneous release of the intact drug [32], [33]. The degradation of this linker does potentially release a quinone methide during the 1,6-elimination step. This species reacts rapidly with water in biological media, and thus a major part of the methide is expected to form p-hydroxy benzyl alcohol (PHBA). It is possible that a small fraction of the methide could react with other nucleophilic groups present in proteins and other biomolecular species. This same methide linker

product is generated with the p-aminobenzyloxycarbonyl (PABC) spacer used widely in clinically approved and safe antibody-drug conjugates. We have also found it safe in initial animal studies using injectable TAF polymer drug depots [13]. If this linker was found to be more of a problem in this long-acting fiber implant, there are alternative linkers that have been described from the antibody-drug conjugate field. The trimethyl lock lactonization chemistry approach, for example, could potentially be used instead of benzyl elimination (BE) to overcome this problem if it becomes a longer-term issue [34].

The drug monomer was synthesized by a five step synthetic route starting from mono-2-(methacryloyloxy)ethyl succinate (SMA) as outlined in Fig. 12. The carboxyl end of SMA was first activated with 2-thiazoline-2-thiol using N,N′-dicyclohexylcarbodimide and 4-(dimethylamino)pyridine (DMAP) and then coupled to p-hydroxybenzyl alcohol (PHB-OH) in the presence of DMAP. Acylation predominantly proceeded at the phenolic hydroxyl group as the phenolate anion generated under basic condition is more nucleophilic than the benzylic hydroxyl group, providing SMA-PHBA (3) (Fig. S1, SI). Phenolic acylation was confirmed by the presence of benzylic hydroxyl signal at 1.75 ppm in ^{1}H NMR spectrum (Fig. S2, SI). 1,1′-Carbonyldimidazole was used to convert the benzylic hydroxyl group of (3) (Fig. S3, SI) into an activated carbonate monomer (4) (Fig. S4, SI), and this step resulted in a downfield shift of benzylic methylene signal from 4.68 to 5.40 ppm. Attempts to conjugate (4) to the amine group on the purine ring of TAF were unsuccessful. A similar approach with 4-nitrophenyl activated carbonate monomer

also failed, indicating that the less nucleophilic purine amine requires a robust acylating reagent for successful conjugation. Hence, a highly reactive N-methylimidazolium triflate quaternized salt monomer was prepared by reacting (4) with methyl trifluoromethanesulfonate following the methods developed by Henry Rapoport [35]. This reactive intermediate (5) underwent the coupling smoothly to give TAF benzyl carbamate monomer (6) in 84% yield. The successful conjugation was confirmed by the carbamate NH signal at 10.64 ppm and an upfield shift of benzyl methylene group from 5.40 to 5.21 ppm in ^{1}H NMR spectrum. TAF purine protons appeared at 8.41 and 8.61 ppm and isopropyl moiety signals were observed at 1.14 and 4.84 ppm. (^{1}H NMR spectra and characterization details are in the Supporting information).

Figure 12: Synthesis of methacrylate based TAF benzyl carbamate monomer.

Polymerizable methacrylate moiety is appended to TAF drug via p-hydroxybenzyloxycarbonyl (PHBC) spacer.

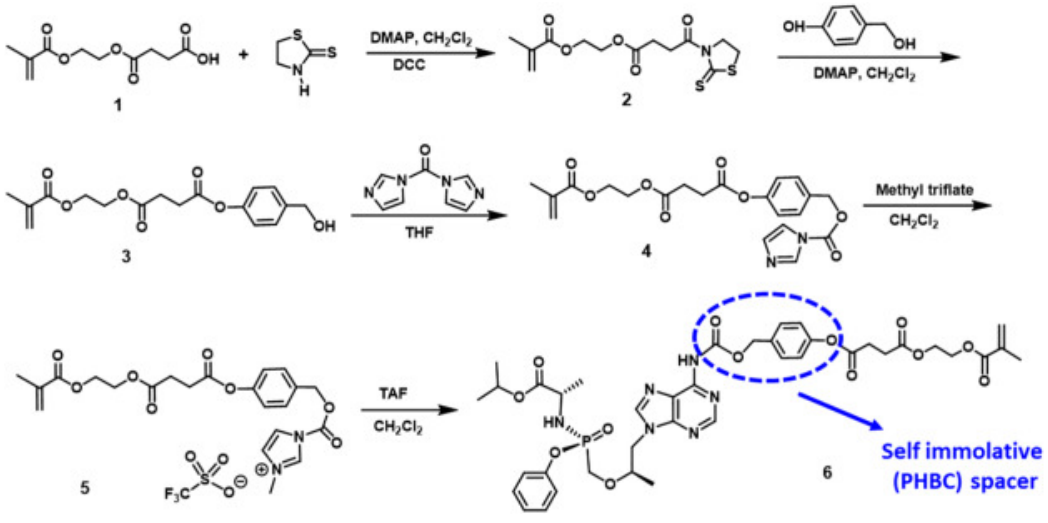

2.4.2 Synthesis and characterization of macro chain transfer agent (pGMA macro CTA) and TAF diblock copolymer

A diblock copolymer of hydrophobic TAF benzyl carbamate methacrylate was synthesized from a hydrophilic glycerol monomethacrylate (GMA) macro chain transfer agent (pGMA macro CTA) using RAFT polymerization (Figure 13) [31]. GMA was chosen as the hydrophilic monomer due to its two hydroxyl groups and relatively low molecular weight which could potentially increase the drug wt% in the final polymer. pGMA macro CTA was synthesized using the molar ratio of [GMA]:[CTA]:[AIBN] = 50/1/0.05 to obtain a relatively short hydrophilic block. To ensure the chain end fidelity, pGMA macro CTA was polymerized up to only 59% monomer conversion. ^{1}H NMR spectrum shows peaks characteristic of pGMA (Fig. S5, SI). Molecular weight and molecular weight distributions of pGMA were determined using GPC (Absolute M_n = 7500 g mol^{-1}, M_w M_n^{-1} = 1.14) (Table 4). Relatively unimodal molecular weight distribution was observed (Fig. 13).

Figure 13: Synthesis of TAF benzyl carbamate diblock copolymer.

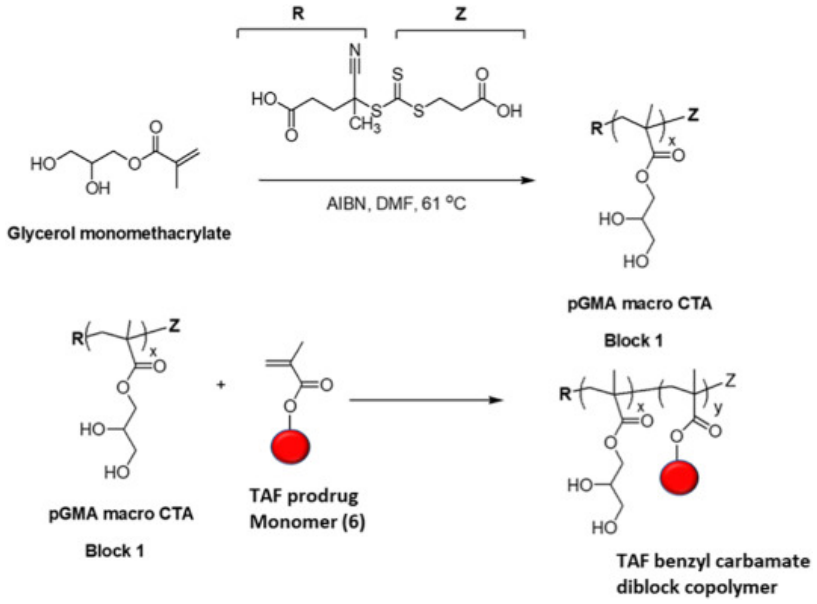

Table 4: Summary of molar feed ratios, molecular weights, molar mass dispersity, monomer and drug wt% for pGMA macro CTA and corresponding di-block copolymer.

Entry	Polymer	[M]:[CTA]:][I] (feed molar ratio)	Monomer conversion[a] (%)	M_n[b] (g mol^{-1})	M_w M_n^{-1}	GMA monomer wt%[a]	TAF monomer wt%[a]	Drug (wt%)[a]
1	pGMA mCTA	50/1/0.05	59	7500	1.14			–
2	TAF di-block copolymer	12/1/0.06	98	19,750	1.16	39.4	60.6	34

[a]As determined by ^{1}H NMR spectroscopy. [b]As determined by gel permeation chromatography (GPC

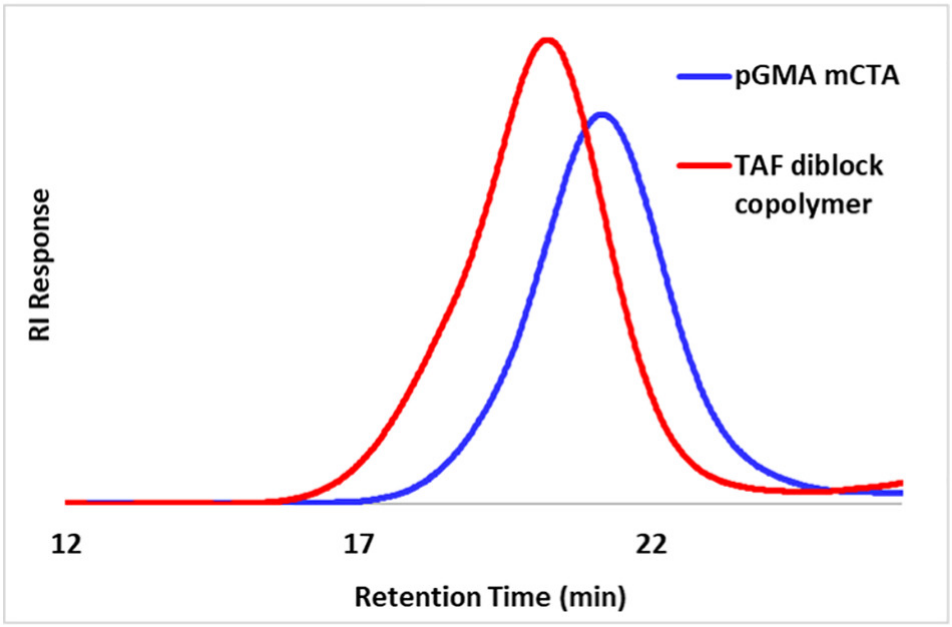

Figure 14: GPC overlays of pGMA macroCTA and TAF diblock copolymer

(eluent: DMF with 0.1% LiBr).

Macro CTA was then chain-extended using the molar ratio of [TAF monomer]:[pGMA mCTA]:[AIBN] = 12/1/0.06. Relatively high monomer conversion was targeted to obtain higher drug loading and to ease the purification of unreacted large TAF monomer. About 98% monomer conversion was obtained in 7.5 h. The polymer was purified via precipitation in diethyl ether and further purified via dialysis against DMSO and cold (4 °C) water. After lyophilization, the polymer was characterized by ^{1}H NMR spectroscopy (Fig. S6, SI) and size exclusion or gel permeation chromatography (SEC/GPC) (Figure 14). The drug wt% of polymer was determined by ^{1}H NMR spectroscopy by comparing the TAF integration at 5.6 ppm with the combined integration of GMA and TAF at 4.8 ppm (Fig. S7, SI). The wt% of GMA, TAF monomer and TAF drug were 39.4%, 60.6% and 34%, respectively. Absolute molecular weight and molecular weight distributions of TAF benzyl carbamate diblock copolymer were determined using GPC (Absolute M_n = 19,750 g mol^{-1}, M_w M_n^{-1} = 1.16). As expected, the GPC peak of diblock copolymer shifted towards higher molecular weight (lower elution time) compared to pGMA macro CTA, suggesting successful chain extension with the TAF benzyl carbamate monomer. Figure 14 shows the GPC overlays of pGMA macro CTA and TAF diblock copolymer. Analysis of the molecular weight and molar mass dispersity of the macro CTA and subsequent chain extension experiments with a clear shift of GPC trace to the lower elution volume suggested the controlled nature of these polymerizations despite the steric bulkiness of the TAF prodrug monomer.

2.4.3 SEM morphological and diameter analysis of PCL and PCL-pTAF fibers

After electrospinning of PCL and PCL-pTAF fibers, samples were observed under field emission SEM. A total of 100 fibers were measured from each sample to determine their average diameter and size distribution. SEM images revealed the topography of both control and PCL-pTAF fibers to be smooth without significant beading or other defects (Figure 15).

Figure 15: SEM images of generated fibers

(A) Control PCL and (B) PCL pTAF fibers.

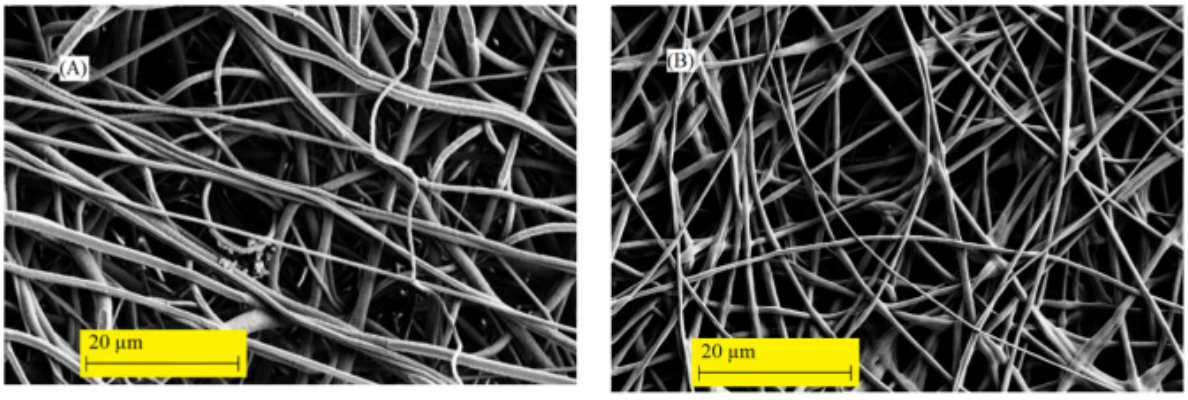

There was, however, a large standard deviation in the diameter of PCL fibers, with a mean diameter of 842 ± 405 nm. Interestingly, the addition of pTAF to the spinning solution reduced both the mean fiber diameter and the standard deviation, (787 ± 212 nm), thus generating more uniform fibers (Figure 16). These results suggest that the addition of pTAF can have a positive effect on generating more high-fidelity fibers for applications where more control over fiber diameter is important [36]. A one-way ANOVA test determined that the

addition of pTAF had a significant effect on fiber diameter compared to the control PCL fibers.

Figure 16: Average diameters for Control PCL (black) and PCL-pTAF ESFs (red) determined from SEM images.

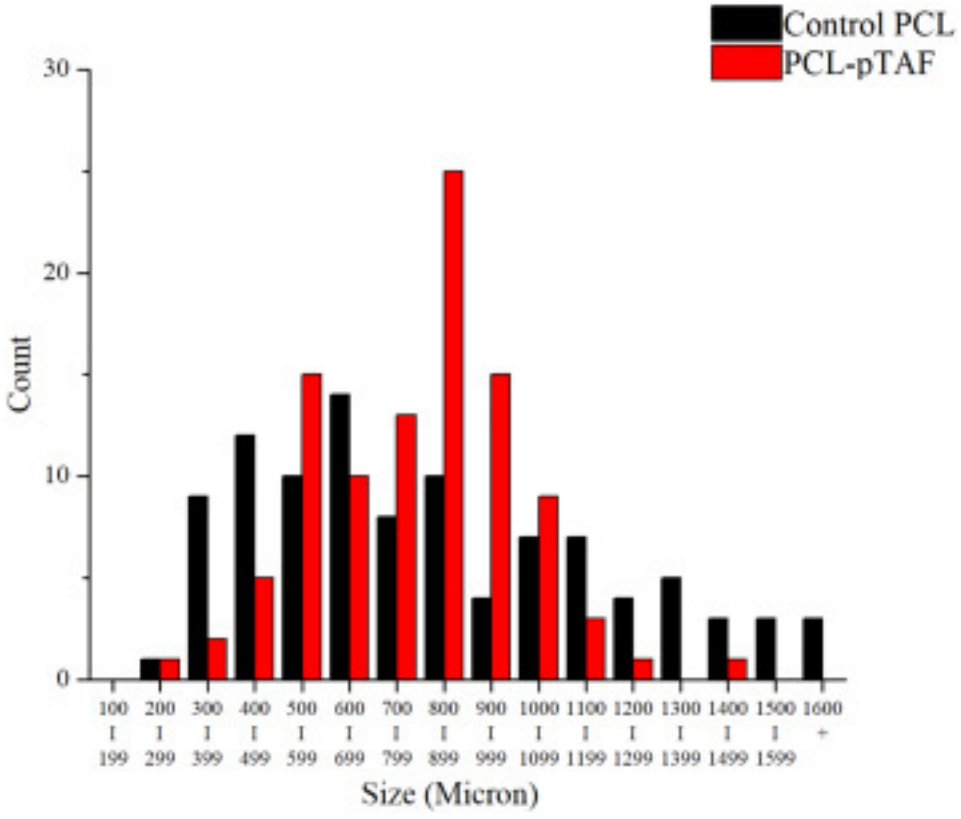

2.4.4 XPS analysis of PCL, PCL-pTAF fibers and pTAF spin coated samples

XPS analysis was performed on all the samples to initially determine the surface elemental composition. Representative survey spectra are shown in Figure 17 and Table 3 shows the elemental composition data generated. The data reveal a clear differentiation between PCL,

PCL-pTAF fibers, and pTAF spin-coated samples. The presence of a nitrogen peak was a clear indication of successful incorporation and surface presentation of pTAF in the fiber samples, as nitrogen is present in pTAF molecule but not PCL.

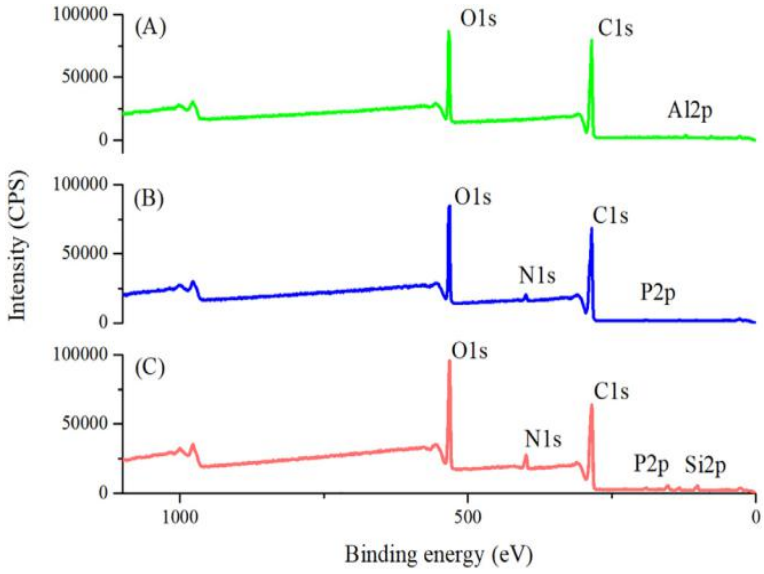

Figure 17: XPS Survey spectra of (A) PCL control fibers, (B) PCL pTAF fibers and (C) pTAF spin-coated samples.

Comparison of the nitrogen composition of spin-coated pure pTAF showed further interesting results when compared to the PCL-pTAF fibers. pTAF consisted of 20% polymer weight of the original solution; thus it was expected that PCL-pTAF fibers would have a nitrogen concentration of ap-proximately 1.0% due to control pTAF spin-coated samples consisting of 5.0 ± 0.3% nitrogen. However, the nitrogen % of ESF pTAF was higher than expected, at 2.2 ± 0.2%, and the surface thickness of pTAF was calcu-lated with the overlayer equation (Eq. (1)) [38].

Table 5: XPS elemental composition of PCL, PCL pTAF fibers and pTAF spin-coated samples.

Element	O %	C %	N %	Si %	P %	Al %
PCL control Fibers	22.9 ± 0.5	76.2 ± 1.3	0.0 ± 0.0	0.0 ± 0.0	0.0 ± 0.0	1.0 ± 0.9
PCL pTAF Fibers	22.8 ± 0.2	74.7 ± 0.3	2.2 ± 0.2	0.0 ± 0.0	0.3 ± 0.2	0.0 ± 0.0
pTAF spin-coated	23.0 ± 1.4	68.8 ± 1.7	5.0 ± 0.4	2.5 ± 0.6	0.8 ± 0.1	0.0 ± 0.0

PCL and PCL-pTAF fibers showed a similar oxygen and carbon content typical for PCL polymers, with control PCL having 76.2 ± 1.3% C, 22.9 ± 0.5% O and PCL-pTAF having 74.7 ± 0.3% C and 22.8 ± 0.2% O (Table 3). The detection of P 2p peaks most likely arises from the presence of phosphorus in the p-hydroxybenzyloxycarbonyl (PHBC) spacer component of pTAF. Low levels of Al and Si contamination were detected on PCL control fibers and pTAF spin-coated samples respectively. Source of the contamination on samples may have come from the underlying Al foil/Si wafer due to a non-uniform of very thin sections of fibers coatings (<10 nm) (Table 3).

Figure 18: High resolution XPS C1s spectra of (A) PCL control fibers (B) PCL pTAF fibers and (C) pTAF spin-coated surface.

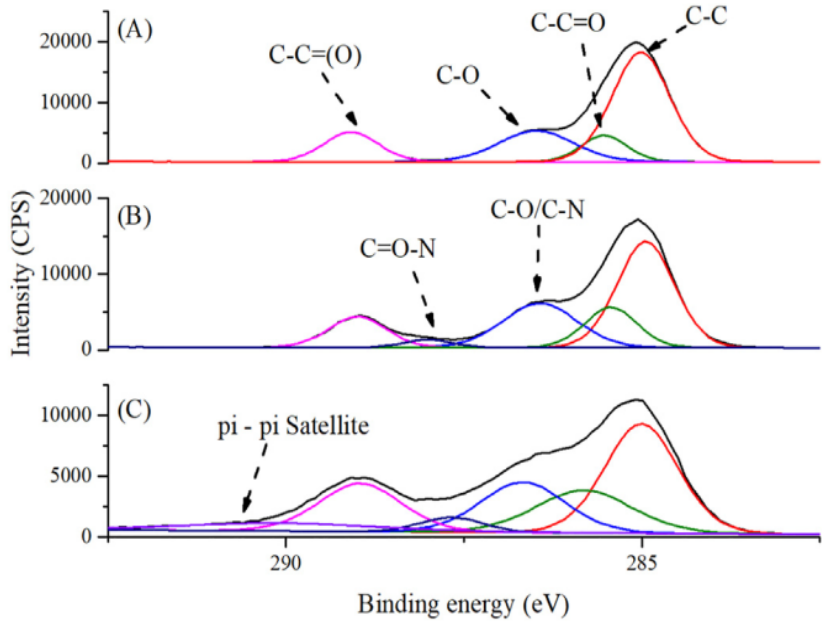

The high resolution XPS C1s spectra for ESF pTAF fibers differed significantly from the control samples. Assignments were made to the C-H/C-C peak at 285.0 eV, the secondary shifted C-C=O peak at 285.5 eV, the CO peak at 286.5 eV and the C=O(O) peak at 289.0 eV for the control PCL fibers, ESF pTAF fibers and pTAF spin coated-surfaces. The PCL-pTAF and spin-coated pTAF additionally had a distinct C=O-N peak at 287.5 eV, and a larger CO peak, which most likely has a contribution from CN environment, further confirming the presence of pTAF at the surface of the fibers (Figure 18).

The high resolution N1s spectra were also acquired and the results also suggest successful incorporation of pTAF at the fiber surface with an identically shaped nitrogen peak detected. The spectra were resolved into three components corresponding to the chemical structure within the pTAF. These include the two C=N-C nitrogen groups from the purine rings at

400.2 eV, one peak at 398.8 eV from the overlapping phosphoryl amino (O=P(O)-N) group and amide (O=C-N) group from TAF linkage to the PHBC spacer [37]. An additional small 402.2 eV shoulder peak was detected that may be part of a positively charged N^+ containing fragment of pTAF. The electrospinning process was unlikely to generate any N^+ containing groups as the spin coated sample also displayed the same shoulder peak (see (6) in Figure 12) (Figure 19).

Figure 19: In vitro release of TFV from PCL-pTAF ESFs.

Tenofovir release from PCL-pTAF in human serum at 37 °C was evaluated by LC-MS/MS. TFV was extracted from serum by precipitating serum proteins with cold methanol. TFV was quantified using TFV calibration curve. The theoretical maximum was calculated as the total mass of TAF incorporated into the ESF. Samples were evaluated in triplicate, with each value representing the mean ± SD (n = 3*). *Day 0 and Day 1 samples had n = 1 due to the limit of detection.

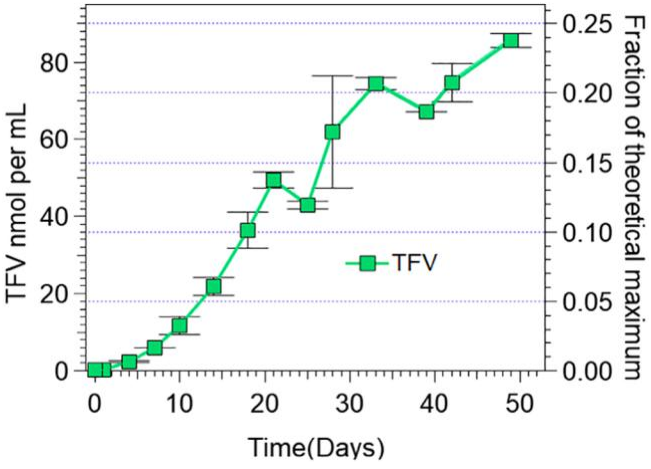

Comparison of the nitrogen composition of spin-coated pure pTAF showed further interesting results when compared to the PCL-pTAF fibers. pTAF consisted of 20% polymer weight of the original solution; thus it was expected that PCL-pTAF fibers would have a nitrogen concentration of approximately 1.0% due to control pTAF spin-coated samples consisting of

5.0 ± 0.3% nitrogen. However, the nitrogen % of ESF pTAF was higher than expected, at 2.2 ± 0.2%, and the surface thickness of pTAF was calcu-lated with the overlayer equation (Eq. (1)) [38].

The overlayer equation to determine the thickness (z) of a layer of material on a given surface

$$z = -\lambda_{IMFP} \times \cos\theta \times \ln\left(1 - \frac{I}{I_\infty}\right)$$

where, z is the thickness of the pTAF surface layer, λ_{IMFP} (2.5 nm) is the in-elastic mean free path of N1s photoelectrons emitted from the sample, θ is estimated to be 57.3° which is the angle between the sample and the analyzer I is the nitrogen signal from PCL-pTAF fibers and I_∞ is the nitrogen signal from pTAF spin coated sample which is assumed infinitely deep.

The thickness was calculated using the PCL-pTAF nitrogen content, when compared that of the spin-coated pTAF surface as that was assumed to be a pure sample. The enrichment of pTAF at the fiber was calculated to have a thickness of 0.783 nm, representing only 0.20% of the total fiber volume. This suggests that although the thickness of pTAF at the surface is thin, pTAF is still concentrated primarily at the outer region of the fiber as opposed to the core of the fiber. The presence of pTAF at the surface of fibers is primarily due to its lower molecular weight and higher hydro-philicity and these factors have been shown to cause surface enrichment in the fiber during blend electrospinning [39,40]. This suggests TAF will be released from the fiber over a sustained period of time since a lot of pTAF is still present in the fiber bulk and PCL

2.4.5 In vitro drug release of pTAF from PCL-pTAF fibers

To evaluate drug release and prolonged delivery efficiency, in vitro release studies of PCL-pTAF ESFs were carried out in human serum; the results are shown in Figure 20. The PCL-pTAF fiber (36.1 mg) composed of TAF 2.45 mg (5.15 μmol) was incubated at 37 °C over 49 days to obtain the release profile. Due to the short half-life of TAF ($t_{1/2}$:117 min) [41] in human plasma and its quick degradation into metabolites such as desphenyl TAF and tenofovir (TFV), TAF released from PCL-pTAF ESFs cannot be directly measured quantitatively. Hence, TAF release was followed by measuring its main metabolite TFV. Because of TAF's 1–2 hour half-life in human serum (similar to plasma), our results cannot distinguish between on-fiber metabolism of TAF to TFV with subsequent release, versus release of TAF and subsequent rapid metabolism to TFV in human serum. Nevertheless, TFV is in its own right an approved HIV antiviral drug, and so long-duration delivery of this species remains relevant in this initial model study.

Isotopically labeled TFV-d_6 was selected as an internal standard to achieve higher quantitative accuracy. The analysis was carried out in negative ESI mode, and TFV and TFV-d_6 were monitored via dual transitions with the most abundant and stable product ions: 285.9 → 110.8, 285.9 → 133.9 for TFV and 291.9 → 110.8, 291.9 → 133.9 for TFV-d_6 as summarized in Table S1 and S2, SI. Calibration standard curves generated with TFV concentration ranging from 8 to 500 ng mL^{-1} were used to quantify TFV release in nmol mL^{-1}, which was then converted into mass fractions. TFV release of 86 ± 2 nmol mL^{-1}, observed over 49 days, accounts for approximately 25% of the incorporated drug in the ESF

pTAF. The theoretical amount of loaded drug was derived from the percentage component of pTAF in the original electrospinning solution multiplied by the weight of the fiber sample used in release testing. The release profile of the TAF metabolite TFV, followed apparent first-order release kinetics over the first 20 days. The sustained TFV release over a 7 week period (49 days) indicates the potential application of PCL-pTAF for controlled and extended release applications. The rate and duration of drug release can be further fine-tuned by molecularly engineering the linker connecting the drug [42], [43], [44], [45], [46]. It is likely that further long term release could be detected with further study.

PCL was used as a model biocompatible polymer scaffold to load with pTAF, however other promising biocompatible polymers systems could also be explored for compatibility with pTAF [25]. In addition, further development of electrospinning incorporating pTAF could result in producing smaller diameter fibers which would further fine-tune the passive release profile of pTAF from the fiber system. Furthermore, it is unclear if the efficacy of the pTAF molecule was affected by the electrospinning process and subsequent release, additional in vivo testing would provide insight to the clinical viability of the described system.

This work has shown nanotherapeutic platforms combined with macroscale drug delivery scaffolds have the potential to be able to deliver sufficient concentrations of antiviral medicine for up to 49 days in vitro, this far exceeds the current half-life of commercial treatments used in daily dose regimens [17]. By incorporating pTAF into an ESF structure, a convenient wearable patch or biodegradable subcutaneous device could be used as a new alternative treatment or preventive option for HIV and hepatitis. This system has the potential to deliver a consistent regimen of medicine, thus reducing the maintenance and upkeep

requirements of treatment plans. These treatment improvements disproportionately have a positive effect on patients with inadequate/inconsistent access to healthcare.

In conclusion, the new prodrug polymer conjugate pTAF was success-fully synthesized via RAFT polymerization, and the prodrug was compatible with PCL in a blend electrospinning system. SEM analyses demonstrated that the addition of pTAF to the spinning solution resulted in most uniform fibers, and XPS analyses revealed that pTAF was overrepresented at the surface of generated fibers. Release in human serum showed a sustained release of pTAF over a period of 49 days suggesting that the scaffold is suitable to deliver a sustained amount of drug over a significant period of time compared to current drug delivery systems that require daily doses in the form of tablets or powder. This technology thus has the potential to provide treatment regimens that are more accessible to a wider population then what is currently available.

2.5 References

Text and Figures were originally published in Dart, A. *et al.* A nanofiber based antiviral (TAF) prodrug delivery system. *Biomaterials Advances* **133**, 112626 (2022).

1 Guvenir, A. Arikan, Hepatitis B virus: from diagnosis to treatment, Pol. J. Microbiol. 69 (4) (2020) 391–399, https://doi.org/10.1016/j.patbio.2010.05.002.

2 A.A.A. Smith, K. Zuwala, M.B.L. Kryger, B.M. Wohl, C. Guerrero-Sanchez, M. Tolstrup, A. Postma, A.N. Zelikin, Macromolecular prodrugs of ribavirin: towards a treatment for co-infection with HIV and HCV, Chem. Sci. 6 (1) (2015) 264–269, https://doi. org/10.1039/C4SC02754J.

3 R. Zampino, A. Boemio, C. Sagnelli, L. Alessio, L.E. Adinolfi, E. Sagnelli, N. Coppola, Hepatitis B virus burden in developing countries, World J. Gastroenterol. 21 (42) (2015) 11941–11953, https://doi.org/10.3748/wjg.v21.i42.11941.

4 A.N. Shaaban, M.R.O. Martins, The importance of improving the quality of care among HIV/AIDS hospitalizations in Portugal, FrontiersPublic Health 7 (266) (2019), https:// doi.org/10.3389/fpubh.2019.00266.

5 A. Quigley, K. O'Brien, R. Parker, M. MacKay-Lyons, Exercise and cognitive function in people living with HIV: a scoping review, Disabil. Rehabil. 41 (12) (2019) 1384–1395, https://doi.org/10.1080/09638288.2018.1432079.

6 L.H. Rubin, P.M. Maki, HIV, depression, and cognitive impairment in the era of effective antiretroviral therapy, Curr. HIV/AIDS Rep. 16 (1) (2019) 82–95, https://doi.org/10. 1007/s11904-019-00421-0.

7 WHO, Global Hepatitis Report, 2017, World Health Organization 2017, 2017.

8 L. Reynaud, M.A. Carleo, M. Talamo, G. Borgia, Tenofovir and its potential in the treat-ment of hepatitis B virus, Ther. Clin. Risk Manag. 5 (1) (2009) 177–185, https://doi. org/10.2147/tcrm.s3335.

9 R. Sampath, J. Zeuli, S. Rizza, Z. Temesgen, Tenofovir alafenamide fumarate for the treatment of HIV infection, Drugs Today 52 (11) (2016) 617–625, https://doi.org/10.1358/dot.2016.52.11.2546852.

10 K. Agarwal, M. Brunetto, W.K. Seto, Y.S. Lim, S. Fung, P. Marcellin, S.H. Ahn, N. Izumi, W.L. Chuang, H. Bae, M. Sharma, H.L.A. Janssen, C.Q. Pan, M.K. Çelen, N. Furusyo, D. Shalimar, K.T. Yoon, H. Trinh, J.F. Flaherty, A. Gaggar, A.H. Lau, A.L. Cathcart, L. Lin, N. Bhardwaj, V. Suri, G.Mani Subramanian, E.J. Gane, M. Buti, H.L.Y. Chan, U.S. Gs, G.-U.-. Investigators, 96 weeks treatment of tenofovir alafenamide vs. tenofovir disoproxil fumarate for hepatitis B virus infection, J. Hepatol. 68 (4) (2018) 672–681, https://doi. org/10.1016/j.jhep.2017.11.039.

11 R.A. Murphy, M.A. Valentovic, Factors contributing to the antiviral effectiveness of te-nofovir, J. Pharmacol. Exp. Ther. 363 (2) (2017) 156–163, https://doi.org/10.1124/jpet.117.243139.

12 H. Wang, X. Lu, X. Yang, N. Xu, The efficacy and safety of tenofovir alafenamide versus tenofovir disoproxil fumarate in antiretroviral regimens for HIV-1 therapy: meta-analysis, Medicine (Baltimore) 95 (41) (2016) e5146, https://doi.org/10.1097/MD. 0000000000005146.

13 D.K. Ho, C. LeGuyader, S. Srinivasan, D. Roy, V. Vlaskin, T.E.J. Chavas, C.L. Lopez, J.M. Snyder, A. Postma, J. Chiefari, P.S. Stayton, Fully synthetic injectable

depots with high drug content and tunable pharmacokinetics for long-acting drug delivery, J. Contr. Rel. 329 (2021) 257–269, https://doi.org/10.1016/j.jconrel.2020.11.030.

14 H. Yang, J. Li, S.K. Patel, K.E. Palmer, B. Devlin, L.C. Rohan, Design of poly(lactic-co-glycolic acid) (PLGA) nanoparticles for vaginal co-delivery of Griffithsin and dapivirine and their synergistic effect for HIV prophylaxis, Pharmaceutics 11 (4) (2019) 184, https://doi.org/10.3390/pharmaceutics11040184.

15 K.M. Tyo, F. Minooei, K.C. Curry, S.M. NeCamp, D.L. Graves, J.R. Fried, J.M. Steinbach-Rankins, Relating advanced electrospun fiber architectures to the temporal release of active agents to meet the needs of next-generation intravaginal delivery applications, Pharmaceutics 11 (4) (2019) 160, https://doi.org/10.3390/pharmaceutics11040160.

16 J. Senapathi, A. Bommakanti, S. Mallepalli, S. Mukhopadhyay, A.K. Kondapi, Sulfonate modified lactoferrin nanoparticles as drug carriers with dual activity against HIV-1, Col-loids Surf. B Biointerfaces 191 (2020), https://doi.org/10.1016/j.colsurfb.2020. 110979.

17 J. das Neves, Novel approaches for the delivery of anti-HIV drugs-what is new? Pharmaceutics 11 (11) (2019) 554, https://doi.org/10.3390/pharmaceutics11110554.

18 N.I. Torres, K.S. Noll, S. Xu, J. Li, Q. Huang, P.J. Sinko, M.B. Wachsman, M.L. Chikindas, Safety, formulation and in vitro antiviral activity of the antimicrobial peptide subtilosin against herpes simplex virus type 1, Probiotics Antimicrob. Proteins 5 (1) (2013) 26–35, https://doi.org/10.1007/s12602-012-9123-x.

19 M. Subic, F. Zoulim, How to improve access to therapy in hepatitis B patients, Liver Int. 38 (2018) 115–121, https://doi.org/10.1007/s12602-012-9123-x.

20 E.T. Overton, G. Richmond, G. Rizzardini, H. Jaeger, C. Orrell, F. Nagimova, F. Bredeek, M.García Deltoro, S. Swindells, J.F. Andrade-Villanueva, A. Wong, M.A. Khuong-Josses, R.Van Solingen-Ristea, V. van Eygen, H. Crauwels, S. Ford, C. Talarico, P. Benn, Y. Wang, K.J. Hudson, V. Chounta, A. Cutrell, P. Patel, M. Shaefer, D.A. Margolis, K.Y. Smith, S. Vanveggel, W. Spreen, Long-acting cabotegravir and rilpivirine dosed every 2 months in adults with HIV-1 infection (ATLAS-2M), 48-week results: a randomised, multicentre, open-label, phase 3b, non-inferiority study, Lancet 396 (10267) (2020) 1994–2005, https://doi.org/10.1016/S0140-6736(20)32666-0.

21 M. Kovarova, S.R. Benhabbour, I. Massud, R.A. Spagnuolo, B. Skinner, C.E. Baker, C. Sykes, K.R. Mollan, A.D.M. Kashuba, J.G. García-Lerma, R.J. Mumper, J.V. Garcia, Ultra-long-acting removable drug delivery system for HIV treatment and prevention, Nat. Commun. 9 (1) (2018) 4156, https://doi.org/10.1038/s41467-018-06490-w.

22 S.M. Simpson, L. Widanapathirana, J.T. Su, S. Sung, D. Watrous, J. Qiu, E. Pearson, A. Evanoff, D. Karunakaran, J.E. Chacon, P.F. Kiser, Design of a drug-eluting subcutaneous implant of the antiretroviral tenofovir alafenamide fumarate, Pharm. Res. 37 (4) (2020) https://doi.org/10.1007/s11095-020-2777-2.

23 K.M. Tyo, A.B. Lasnik, L. Zhang, M. Mahmoud, A.B. Jenson, J.L. Fuqua, K.E. Palmer, J.M. Steinbach-Rankins, Sustained-release Griffithsin nanoparticle-fiber

composites against HIV-1 and HSV-2 infections, J. Control. Release 321 (2020) 84–99, https:// doi.org/10.1016/j.jconrel.2020.02.006.

24 N.S. Malik, M. Ahmad, M.U. Minhas, R. Tulain, K. Barkat, I. Khalid, Q. Khalid, Chitosan/ xanthan gum based hydrogels as potential carrier for an antiviral drug: fabrication, characterization, and safety evaluation, Front. Chem. 8 (2020), https://doi.org/10. 3389/fchem.2020.00050.

25 A. Dart, M. Bhave, P. Kingshott, Antimicrobial peptide-based electrospun fibers for wound healing applications, Macromol. Biosci. 019 (0) (2019), 1800488, https:// doi.org/10.1002/mabi.201800488.

26 R.K. Thapa, D.B. Diep, H.H. Tønnesen, Topical antimicrobial peptide formulations for wound healing: current developments and future prospects, Acta Biomater. 103 (2020) 52–67, https://doi.org/10.1016/j.actbio.2019.12.025.

27 M. Chen, M. Dong, R. Havelund, V.R. Regina, R.L. Meyer, F. Besenbacher, P. Kingshott, Thermo-responsive core-sheath electrospun nanofibers from poly (N-isopropylacrylamide)/polycaprolactone blends, Chem. Mater. 22 (14) (2010) 4214–4221, https://doi.org/10.1021/cm100753r.

28 E. Malikmammadov, T.E. Tanir, A. Kiziltay, V. Hasirci, N. Hasirci, PCL and PCL-based materials in biomedical applications, J. Biomater. Sci. Polym. Ed. 29 (7–9) (2018) 863–893, https://doi.org/10.1080/09205063.2017.1394711.

29 R.T.A. Mayadunne, E. Rizzardo, J. Chiefari, Y.K. Chong, G. Moad, S.H. Thang, Living radical polymerization with reversible addition-fragmentation chain transfer

(RAFT po-lymerization) using dithiocarbamates as chain transfer agents, Macromolecules 32 (21) (1999) 6977–6980, https://doi.org/10.1021/ma9906837.

30 R.B. Greenwald, A. Pendri, C.D. Conover, H. Zhao, Y.H. Choe, A. Martinez, K. Shum, S. Guan, Drug delivery systems employing 1,4- or 1,6-elimination: poly(ethylene glycol) prodrugs of amine-containing compounds, J. Med. Chem. 42 (18) (1999) 3657–3667, https://doi.org/10.1021/jm990166e.

31 J. Noh, B. Kwon, E. Han, M. Park, W. Yang, W. Cho, W. Yoo, G. Khang, D. Lee, Am-plification of oxidative stress by a dual stimuli-responsive hybrid drug enhances cancer cell death, Nat. Commun. 6 (6907) (2015), https://doi.org/10.1038/ncomms7907.

32 B.E. Watkins, J.S. Kiely, H. Rapoport, Synthesis of oligodeoxyribonucleotides using N-benzyloxycarbonyl-blocked nucleosides, J. Am. Chem. Soc. 104 (21) (1982) 5702–5708, https://doi.org/10.1021/ja00385a026.

33 A. Haider, S. Haider, I.K. Kang, A comprehensive review summarizing the effect of electrospinning parameters and potential applications of nanofibers in biomedical and biotechnology, Arab. J. Chem. 11 (8) (2015) 1165–1188, https://doi.org/10.1016/j.arabjc.2015.11.015.

34 L. Bildstein, C. Dubernet, P. Couvreur, Prodrug-based intracellular delivery of antican-cer agents, Adv.Drug Deliv. Rev. 63 (1–2) (2011) 3–23, https://doi.org/10.1016/j. addr.2010.12.005.

35 D. G.B. Beamson, High resolution XPS of organic polymers: the Scienta ESCA300 data-base, Journal of Chemical Education 70 (1) (1993), A25, https://doi.org/10.1021/ed070pA25.5.

36 R.W. Paynter, B.D. Ratner, T.A. Horbett, H.R. Thomas, XPS studies on the organization of adsorbed protein films on fluoropolymers, J. Colloid Interface Sci. 101 (1) (1984) 233–245, https://doi.org/10.1016/0021-9797(84)90023-7.

37 M. Wang, D. Fang, N. Wang, S. Jiang, J. Nie, Q. Yu, G. Ma, Preparation of PVDF/PVP core–shell nanofibers mats via homogeneous electrospinning, Polymer 55 (9) (2014) 2188–2196, https://doi.org/10.1016/j.polymer.2014.02.035.

38 J.-F. Zhang, D.-Z. Yang, F. Xu, Z.-P. Zhang, R.-X. Yin, J. Nie, Electrospun core−shell structure nanofibers from homogeneous solution of poly(ethylene oxide)/chitosan, Macromolecules 42 (14) (2009) 5278–5284, https://doi.org/10.1021/ma900657y.

39 D. Babusis, T.K. Phan, W.A. Lee, W.J. Watkins, A.S. Ray, Mechanism for effective lym-phoid cell and tissue loading following oral administration of nucleotide prodrug GS-7340, Mol. Pharm. 10 (2) (2013) 459–466, https://doi.org/10.1021/mp3002045.

40 D. Das, S. Srinivasan, A.M. Kelly, D.Y. Chiu, B.K. Daugherty, D.M. Ratner, P.S. Stayton, A.J. Convertine, RAFT polymerization of ciprofloxacin prodrug monomers for the con-trolled intracellular delivery of antibiotics, Polym. Chem. 7 (4) (2016) 826–837, https://doi.org/10.1039/c5py01704a.

41 H.N. Son, S. Srinivasan, J.Y. Yhee, D. Das, B.K. Daugherty, G.Y. Berguig, V.G. Oehle, S.H. Kim, K. Kim, I.C. Kwon, P.S. Stayton, A.J. Convertine,

Chemotherapeutic copoly-mers prepared: via the RAFT polymerization of prodrug monomers, Polym. Chem. 7 (27) (2016) 4494–4505, https://doi.org/10.1039/c6py00756b.

42 M. Danial, A.H.F. Andersen, K. Zuwala, S. Cosson, C.F. Riber, A.A.A. Smith, M. Tolstrup, G. Moad, A.N. Zelikin, A. Postma, Triple activity of lamivudine releasing sulfonated polymers against HIV-1, Mol. Pharm. 13 (7) (2016) 2397–2410, https://doi.org/10. 1021/acs.molpharmaceut.6b00156.

43 F.Y. Su, S. Srinivasan, B. Lee, J. Chen, A.J. Convertine, T.E. West, D.M. Ratner, S.J. Skerrett, P.S. Stayton, Macrophage-targeted drugamers with enzyme-cleavable linkers deliver high intracellular drug dosing and sustained drug pharmacokinetics against alveolar pulmonary infections, J. Control. Release 287 (2018) 1–11, https://doi.org/10.1016/j.jconrel.2018.08.014.

44 D. Das, S. Srinivasan, F.D. Brown, F.Y. Su, A.L. Burrell, J.M. Kollman, A. Postma, D.M. Ratner, P.S. Stayton, A.J. Convertine, Radiant star nanoparticle prodrugs for the treat-ment of intracellular alveolar infections, Polym. Chem. 9 (16) (2018) 2134–2146, https://doi.org/10.1039/c8py00202a.

45 M. Abrigo, P. Kingshott, S.L. McArthur, Bacterial response to different surface chemis-tries fabricated by plasma polymerization on electrospun nanofibers, Biointerphases 10 (4) (2015) 1–9, https://doi.org/10.1116/1.4927218.

46 P. Louette, F. Bodino, J.J. Pireaux, Pireaux Poly(caprolactone) (PCL) XPS Reference Core Level and Energy Loss Spectra, 12(1), 2005, pp. 27–31, https://doi.org/10.1116/11.20050906

3 Polymeric pro-drug delivery targeting Pseudomonas biofilm

3.1 Abstract

Biofilms are one of the most challenging obstacles in bacterial infection. By providing protection against immune responses and antibiotic therapies, biofilms enable chronic colonization and the development of antibiotic resistance. As previous clinical observations and studies have shown, traditional antibiotic therapy alone cannot effectively treat and eliminate biofilm forming infections[1]. A new treatment mode specifically developed against biofilms must be developed. Here, we specifically target and bind to the PAO1 biofilm and elucidate the molecular mechanism behind the interaction between a glycosylated polymeric delivery vehicle and biofilm using a continuous flow biofilm model. Incubation of biofilms with fluorescent delivery vehicles demonstrated strong and persistent interactions with the mannose-containing polymer, even after 24 hours of continuous flow. To evaluate the role of major biofilm proteins Lec B and CdrA, loss of function experiments with knockout variants established the dual involvement of both proteins in mannosylated polymer retention. These results identify a persistent and specific targeting strategy to the biofilm, emphasizing its potential value as a delivery strategy and encouraging further exploration of biofilm targeted delivery.

3.2 Literature Review

Biofilms are microbial aggregates composed of bacteria and extracellular matrices including exopolysaccharides (EPS), extracellular DNA (eDNA), and proteins[2-4]. The matrix serves as a structural scaffold for these communities and also protects against host immune responses and antimicrobials [5-7]. Biofilm formation contributes to *P. aeruginosa* infections of burns, chronic wounds, and implanted medical devices [2,8-10]. Biofilm aggregates also contribute to chronic airway infections in patients with CF [11,12]. Among other factors, the accumulation of mucus in the airways of these patients is believed to create an environment that encourages biofilm development, and biofilm aggregates of *Pseudomonas aeruginosa* (*Pa*) have been observed in the expectorated sputum of CF patients [13-15].

Successful treatment of biofilm infections often requires physical disruption of the biofilms and sustained concentrations of antibiotics. Treatment of pulmonary *Pseudomonas* infections is limited by the systemic dissemination of current antimicrobial drugs. This contributes to off-target effects and possible antimicrobial resistance[16-18]. Pulmonary administration of antimicrobials has the potential to improve over intravenous therapy by maximizing delivery to the site of infection and reducing adverse reactions. However, the *Pseudomonas* biofilm confers phenotypic resistance and decreases antibiotic susceptibility[19]. Once airway colonization is established, successful treatment and eradication of *Pa* infections is challenging[19]. To improve efficacy and reduce treatment burden, biofilm specific delivery methods must be developed. Here, we demonstrate a novel targeting strategy based on synthetic polymeric prodrugs that incorporate carbohydrate moieties capable of targeting and binding to the *Pa* biofilm.

Pa biofilm matrices can contain two different EPS: Pel and Psl. Pel is composed of the monosaccharides N-acetylglucosamine (GlcNAc) and N-acetyl galactosamine (GalNAc), while Psl is composed of a repeating pentasaccharide subunit that contains mannose, rhamnose, and glucose in a 3:1:1 ratio[20-23]. Currently, two proteins, CdrA and LecB, are known to interact with Psl and contribute to biofilm structural integrity and maintenance [24,31]. CdrA is a cell associated and secreted 150 kDa adhesin (*cdrA* gene encodes a 220-kDa protein and CdrA is processed to 150 kDa) predicted to contain sugar binding and carbohydrate-dependent hemagglutination domains[24]. CdrA binds to Psl, promoting aggregation in liquid culture, which can be blocked by the addition of mannose to the growth medium [24]. Additionally, CdrA promotes the tight association of Psl to the biofilm aggregate periphery[24]. Recently, it was demonstrated that CdrA also can promote aggregate formation even in the absence of Psl via CdrA-CdrA interactions[25]. LecB is a 12 kDa soluble lectin associated with the outer membrane. The ability of LecB to bind fucose and mannose confers a dual role in pathogenesis[26-28]. First, LecB aids in bacterial adhesion through interactions with mammalian mucins present in the accumulated mucus, which is rich in fucose[26,29]. LecB also plays a role in biofilm formation due to its affinity towards mannose present in Psl [30,31]. Recently, it was shown that LecB coordinates Psl placement in the periphery of the aggregate, which is a crucial step for biofilm maturation[31]. Thus, the evidence supports that both CdrA and LecB bind to Psl and can promote Psl localization at the biofilm aggregate periphery.

Polymeric delivery vehicles represent an exciting alternative to traditional drug formulations. Enabled by synthetic methods and polymer chemistry, polymeric vehicles are modular

multifunctional systems that facilitate precise control of macromolecular properties through variation in monomer composition. Prior developments have demonstrated the utility of this modular strategy since it enables the incorporation of a wide array of monomers, including cleavable linkers (including enzyme cleavable), drugs, and functional elements conferring targeting, solubility, and biocompatibility[32-34]. Reversible addition-fragmentation chain transfer (RAFT) polymerization permits precise control of polymer composition, size, and structure Additionally, RAFT polymer chemistry is compatible with both organic and aqueous conditions, obviating the need for complex protecting group chemistries. Previously, we have leveraged these beneficial features of RAFT to synthesize a variety of polymeric delivery vehicles, including unimeric, diblock miscelle-forming, and radiant star polymers[32,35,36].

In this study, we used a mannose ciprofloxacin polymeric delivery vehicle (Man-polymer). This polymer was previously explored for use in alveolar macrophage targeting, demonstrating *in vivo* efficacy in treating a murine model of *Francisella* infection[33-35]. As illustrated in Scheme 1, the Man-polymer and galactose polymeric delivery vehicle (Gal-polymer) include: (1) a rhodamine monomer to allow tracking of the polymers, (2) either mannose ethyl methacrylate or galactose ethyl methacrylate carbohydrate monomers for targeting and biocompatibility, and (3) an example therapeutic cargo of ciprofloxacin prodrug monomers. Mannose and galactose, two aldohexose monosaccharide epimers, represent a useful carbohydrate pairing as they have the same molecular weight and differ only in the stereochemistry of the pendant hydroxyl moieties. The pharmacokinetics of antibiotic release, biodistribution, and efficacy of similar polymeric delivery vehicles were previously characterized[34,35]. These prior studies established the strategy

to synthesize functional polymeric systems capable of targeting endogenous carbohydrate-binding proteins and receptors. Here we leverage that capability to demonstrate targeting and elaborate the mechanism of functional polymer binding to the biofilm of the PAO1 *Pseudomonas* strain (Figure 21)

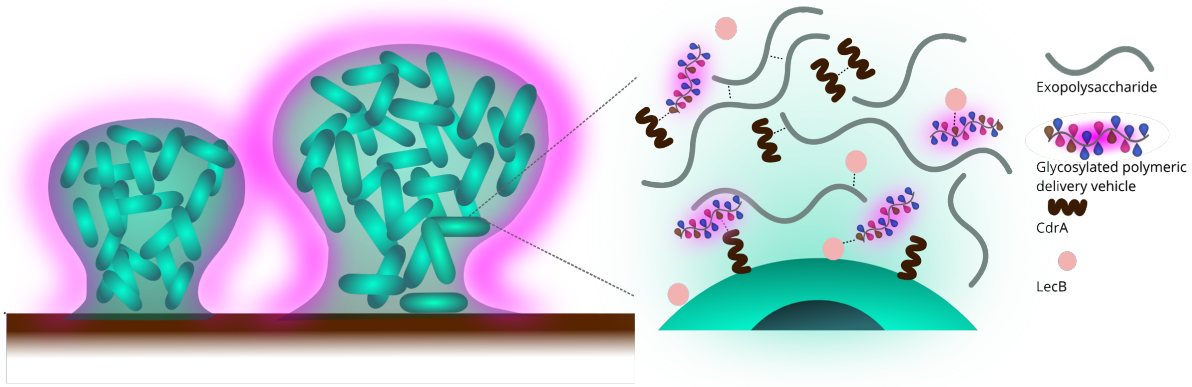

Figure 21: Model of possible *Pseudomonas* biofilm interactions with Man-polymer via CdrA and LecB in the periphery of the PAO1 aggregates.

The model shows the aggregates (green) with peripheral rhodamine fluorescence (magenta) from the polymeric delivery vehicles. The magnified insert shows the polymeric delivery vehicles interacting with CdrA (brown) and LecB (peach) within the biofilm exopolysaccharide matrix (gray)

3.3 Methodology

3.3.1 Polymer synthesis

Briefly, ciprofloxacin prodrug monomers with phenyl ester linkers were synthesized and purified following published protocols[32,34,35]. Other materials, including the monomers mannose

ethylmethacrylate, galactose ethylmethacrylate, and rhodamine methacrylate was synthesized as previously described[34]. RAFT polymerization of the polymeric delivery vehicle containing rhodamine methacrylate, hydrolyzable ciprofloxacin monomer, and either the mannose or galactose ethylmethacrylate monomer was performed in acetate buffer at a 4.3 mM:121 mM:964 mM ratio (rhodamine : ciprofloxacin : glycan) under a nitrogen atmosphere using 4-cyano-4-(phenylcarbonothioylthio) pentanoic acid as the chain transfer agent and ABCVA as the radical initiator[35]. Both polymers were previously characterized and described[35].

3.3.2 Bacterial methods

The PAO1 *Pa* strains used in this study were propagated at 37°C in Tryptic Soy Broth (TSB; Difco). Continuous flow cell biofilm reactors were prepared and assembled as previously described[37]. Bacteria were grown in TSB to log phase and then diluted in 1% TSB to a final OD_{600} of 0.01. Flow cell chambers were inoculated and incubated inverted for 1 h. Then flow was initiated, and the bacteria were continuously supplied with fresh 1% TSB at 10 mL/h.

To assess binding and specificity for glycosylated polymers, four-day-old biofilms were treated with the Man-polymer or Gal-polymer at 30 μg/mL statically for 30 min (flow was suspended during this incubation period). Following static incubation with the polymers, flow was restored at 10 mL/h for periods ranging from 5 minutes to 24 hours to rinse unbound polymers and interrogate retention by the biofilm. Biomasses were stained with 2.5 μM Syto62 (Molecular Probes) before imaging with a Zeiss LSM 510 confocal laser scanning microscope. Volocity

software (Improvision) was used to compile and quantify image series using the same parameters previously described[31].

3.4 Results & Discussion

To assess the interaction of the glycan-modified vehicles with the *Pa* biofilms, *Pa* aggregates were statically incubated with either Man- or Gal-polymers prior to restoring flow to remove unbound polymer. The same Man-polymer and Gal-Polymer vehicles were previously used to study carbohydrate-specific targeting of endogenous receptors on the alveolar macrophage[32].

By comparing the interaction of the Man- and Gal-polymer with the *Pa* biofilm, as measured by the fluorescence due to the copolymerized rhodamine monomer, it is possible to determine whether there is a specific carbohydrate-dependent interaction between the biofilm and the polymeric vehicle as a result of the incorporated glycans. As evidenced by the results illustrated in Figure 2, there was a marked contrast between the interaction of the Man- and Gal-polymers with the *Pa* biofilm aggregates. The Man-polymer demonstrated significant binding to the periphery of the PAO1 aggregates (Figure 22B), whereas the Gal-polymer demonstrated no observable interaction with the biofilm (Figure 22E). As an additional control, we also examined the binding of a non-carbohydrate-containing polymer based on a zwitterionic carboxybetaine-containing monomer, and no appreciable binding to the biofilm was observed (data not shown).

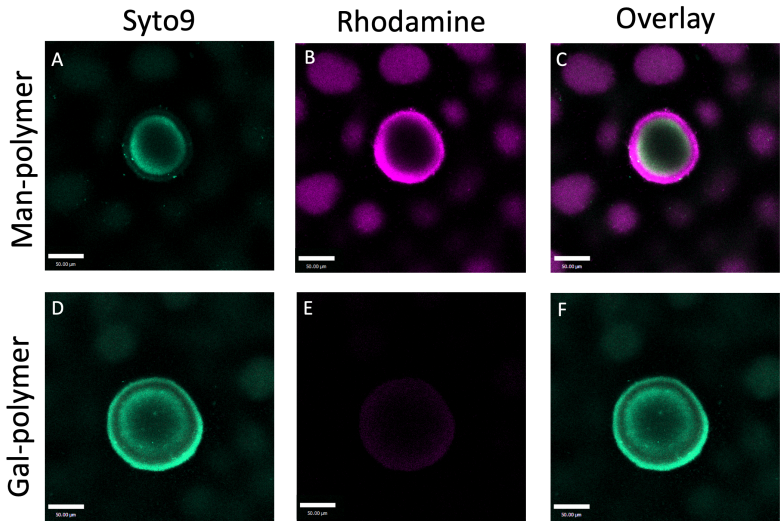

Figure 22: Specificity of Man-polymer for PAO1 biofilms.

Cultured PAO1 biofilms were treated with Man-polymer (A, B, C) and Gal-polymer (D, E, F). Syto9 staining for biomass shows that characteristic aggregate formed (green, A, D). Rhodamine fluorescence of the Man- and Gal-polymers shows strong peripheral binding of Man-polymers (magenta, B) but not Gal-polymers(E). Overlay of Syto9 staining and rhodamine fluorescence signal reveals peripheral localization of Man-polymers(C) but not Gal-polymers(F). The scale bar indicates 50 μm.

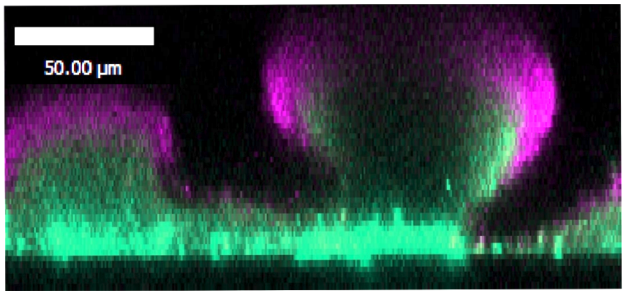

Figure 23: Peripheral binding of Man-polymer to PAO1 aggregates

Binding is evident in the optical cross-section of z-stacked images. Rhodamine fluorescence from Man-polymer (magenta) is localized in the periphery of the aggregates (Syto9, green), which is similar to the peripheral localization of Psl.

As shown in Figure 23, the Man-polymer localizes to the periphery of the aggregates. This finding combined with the robust retention of the polymers led us to hypothesize that the Man-polymer may be retained by the matrix proteins LecB and CdrA. As illustrated in the schematic in Figure 21, LecB and CdrA are known to bind to the mannose containing Psl and also promote Psl localization to the biofilm aggregate periphery [1,31].

To establish the stability of the biofilm retention of the Man-polymer, the biofilms were incubated with the Man- and Gal-polymers (30 μg/mL; 30 min), and then subjected to continuous flow of growth media. We examined the fluorescence in the biofilms to determine if the glycosylated polymers were retained over a 24-hour period. As illustrated in Figure 24, the Man-polymer shows peripheral binding to the biofilm aggregate at 5-minutes post-incubation, and this binding is retained with minimal loss of fluorescence intensity after 24-hours of continuous flow of growth media (Figure 24B). By contrast, the Gal-polymer shows no detectable binding to the biofilm aggregates. These results demonstrate a robust interaction between the Man-Polymer and the biofilm, suggesting a high-avidity multivalent interaction between the glycosylated polymer and the biofilm matrix.

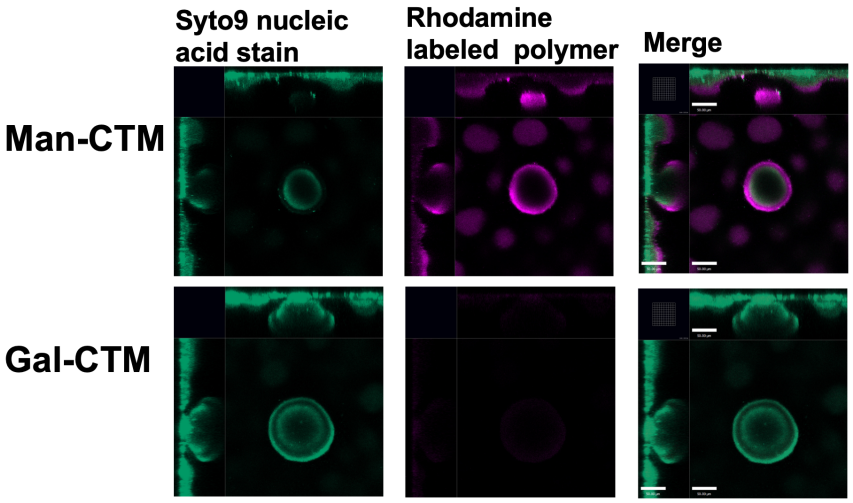

Figure 24. Specificity of mannose drugamer for PAO1 biofilms.

Cultured PAO1 biofilms were treated with either the mannose (Man-CTM, A, B, C) or galactose (Gal-CTM, D, E, F) drugamer. The biomass staining shows characteristic aggregate structure (green, Syto9, A, D). Fluorescence from the Mannose and Galactose drugamers shows strong peripheral binding of the Mannose drugamer (magenta, Rhodamine, B) but not the Gal drugamer (E). The overlay of Syto9 staining and rhodamine fluorescence signal reveals peripheral localization of the biomass and the mannose drugamer (C) but not the galactose drugamer (F)

Due to the enhanced retention of the polymeric system within the biofilm, these long-lived interactions support the possibility of applying these findings in drug delivery applications where continuous and sustained release of drug from a retained polymeric delivery vehicle could support a novel therapeutic strategy with significant benefits over traditional pulmonary delivery of small molecules. While the continuous flow of TBS essential to generate the characteristic *Pseudomonas* phenotype precluded the ability to perform any efficacy or extended pharmacokinetics studies, our previous work with similar delivery vehicles demonstrated great efficacy in pulmonary infection models and established controlled drug release profiles, with

zero-order drug release profiles demonstrated over a period of hours to weeks, and efficacy against multiple pulmonary pathogens [35].

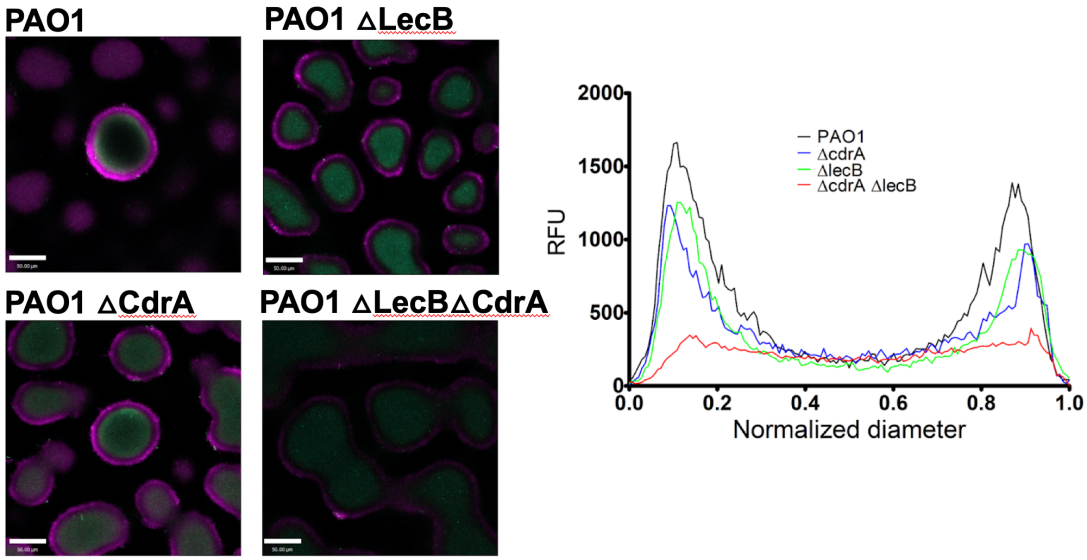

Figure 25. Knockout experiments illustrate the role of LecB and CdrA in binding the Mannose drugamer.

PAO1 (A1) shows the characteristic aggregate shape and strong peripheral Man-drugamer binding. Aggregates from PAO1 Δ*lecB* (A2) and Δ*cdrA* (3) single knockouts retain characteristic peripheral binding morphology and similar rhodamine fluorescence and retention. The Δ*lecB* Δ*cdrA* (A4) knockout showed dramatically reduced Man-drugamer binding and altered biomass structure, consistent with our understanding of the roles of CdrA and LecB in the PA biofilm. Line profile (B) of rhodamine fluorescence from the mannose drugamer.

Since Psl is known to interact with two mannose binding proteins, CdrA and LecB, we postulated that the mannose-specific binding and prolonged retention of the polymer was due to one or both of these proteins[25,31]. To test this hypothesis, we initially evaluated the retention of Man-polymer by biofilms formed from the single knockout mutants PAO1 Δ*cdrA* and PAO1

Δ*lecB*. As illustrated in Figure 25, Man-polymer retention was only slightly diminished by the loss of either *cdrA* or *lecB* and peripheral retention was clearly observed (Figure 25B and 25C). This result suggests that loss of a single protein, either CdrA or LecB, would not necessarily eliminate biofilm retention of the polymeric vehicle. However, biofilms formed by the double mutant PAO1 Δ*cdrA* Δ*lecB* did not retain the Man-polymer, and only a diffuse and faint fluorescent signal of the Man-polymer was observed (Figure 25D and 25E). These results suggest that CdrA and LecB both are likely involved in the peripheral retention of the Man-polymer. However, it is not clear if the reduced polymer retention is the result of the lack of CdrA and LecB or the reduced biomass in the PAO1 Δ*cdrA* Δ*lecB aggregates*.

As shown in this study, the carbohydrate-specific targeting of *Pa* biofilms via glycosylated polymer a novel strategy for biofilm targeting. This strategy could allow for the extended retention of polymeric delivery vehicles and sustained release of therapeutic cargo within the biofilm. Our understanding of the *Pa* biofilm supports a biochemical explanation for the specificity of targeting. While the system used in this study precluded efficacy studies, our results strongly suggest the potential of mannose targeting to support delivery of drug or therapeutic systems to *Pa* biofilm infections and highlight the need for future efficacy studies in more suitable models. The ability to synthetically construct multifunctional polymers capable of the facile incorporation of targeting moieties and therapeutic cargo makes it possible to engineer custom polymeric delivery vehicles to address the unique challenges of the infection setting.

3.5 References

Text and Figures were originally published in Limqueco, E. *et al.* Mannose Conjugated Polymer Targeting *P. aeruginosa* Biofilms. *ACS Infect. Dis.* **6**, 2866–2871 (2020).

1 Wu, H., Moser, C., Wang, H. Z., Hoiby, N. & Song, Z. J. Strategies for combating bacterial biofilm infections. *Int J Oral Sci* **7**, 1-7, doi:10.1038/ijos.2014.65 (2015).

2 Bjarnsholt, T. *et al.* The in vivo biofilm. *Trends Microbiol* **21**, 466-474, doi:10.1016/j.tim.2013.06.002 (2013).

3 Costerton, J. W. Bacterial Biofilms: A Common Cause of Persistent Infections. *Science* **284**, 1318-1322, doi:10.1126/science.284.5418.1318 (1999).

4 Hall-Stoodley, L., Costerton, J. W. & Stoodley, P. Bacterial biofilms: from the natural environment to infectious diseases. *Nat Rev Microbiol* **2**, 95-108, doi:10.1038/nrmicro821 (2004).

5 Anderl, J. N., Franklin, M. J. & Stewart, P. S. Role of Antibiotic Penetration Limitation in Klebsiella pneumoniae Biofilm Resistance to Ampicillin and Ciprofloxacin. *Antimicrobial Agents and Chemotherapy* **44**, 1818-1824 (2000).

6 Doroshenko, N. *et al.* Extracellular DNA impedes the transport of vancomycin in Staphylococcus epidermidis biofilms preexposed to subinhibitory concentrations of vancomycin. *Antimicrob Agents Chemother* **58**, 7273-7282, doi:10.1128/AAC.03132-14 (2014).

7 Tseng, B. S. *et al.* The extracellular matrix protects Pseudomonas aeruginosa biofilms by limiting the penetration of tobramycin. *Environ Microbiol* **15**, 2865-2878, doi:10.1111/1462-2920.12155 (2013).

8 Gbejuade, H. O., Lovering, A. M. & Webb, J. C. The role of microbial biofilms in prosthetic joint infections. *Acta Orthop* **86**, 147-158, doi:10.3109/17453674.2014.966290 (2015).

9 Kennedy, P., Brammah, S. & Wills, E. Burns, biofilm and a new appraisal of burn wound sepsis. *Burns* **36**, 49-56, doi:10.1016/j.burns.2009.02.017 (2010).

10 Stickler, D. J. Bacterial biofilms and the encrustation of urethral catheters. *Biofouling* **9**, 293-305, doi:10.1080/08927019609378311 (1996).

11 Singh, P. K. *et al.* Quorum-sensing signals indicate that cystic fibrosis lungs are infected with bacterial biofilms. *Nature* **407**, 762-764 (2000).

12 Kragh, K. N. *et al.* Polymorphonuclear leukocytes restrict growth of Pseudomonas aeruginosa in the lungs of cystic fibrosis patients. *Infect Immun* **82**, 4477-4486, doi:10.1128/IAI.01969-14 (2014).

13 Staudinger, B. J. *et al.* Conditions associated with the cystic fibrosis defect promote chronic Pseudomonas aeruginosa infection. *Am J Respir Crit Care Med* **189**, 812-824, doi:10.1164/rccm.201312-2142OC (2014).

14 Foundation, C. F. Cystic Fibrosis Foundation Patient Registry 2008 annual data report. . *Cystic Fibrosis Foundation, Bethesda, MD* (2009).

15 Sonderholm, M. *et al.* Pseudomonas aeruginosa Aggregate Formation in an Alginate Bead Model System Exhibits In Vivo-Like Characteristics. *Applied and Environmental Microbiology* **83**, doi:10.1128/ (2017).

16 Kalil, A. C. *et al.* Management of Adults With Hospital-acquired and Ventilator-associated Pneumonia: 2016 Clinical Practice Guidelines by the Infectious Diseases Society of America and the American Thoracic Society. *Clin Infect Dis* **63**, e61-e111, doi:10.1093/cid/ciw353 (2016).

17 Golomb, B. A., Koslik, H. J. & Redd, A. J. Fluoroquinolone-induced serious, persistent, multisymptom adverse effects. *BMJ Case Rep* **2015**, doi:10.1136/bcr-2015-209821 (2015).

18 Krause, K. M., Serio, A. W., Kane, T. R. & Connolly, L. E. Aminoglycosides: An Overview. *Cold Spring Harb Perspect Med* **6**, doi:10.1101/cshperspect.a027029 (2016).

19 Flume, P. A. *et al.* Continuous alternating inhaled antibiotics for chronic pseudomonal infection in cystic fibrosis. *J Cyst Fibros* **15**, 809-815, doi:10.1016/j.jcf.2016.05.001 (2016).

20 Byrd, M. S. *et al.* Genetic and biochemical analyses of the Pseudomonas aeruginosa Psl exopolysaccharide reveal overlapping roles for polysaccharide synthesis enzymes in Psl and LPS production. *Mol Microbiol* **73**, 622-638, doi:10.1111/j.1365-2958.2009.06795.x (2009).

21 Jackson, K. D., Starkey, M., Kremer, S., Parsek, M. R. & Wozniak, D. J. Identification of psl, a locus encoding a potential exopolysaccharide that is essential for Pseudomonas

aeruginosa PAO1 biofilm formation. *J Bacteriol* **186**, 4466-4475, doi:10.1128/JB.186.14.4466-4475.2004 (2004).

22 Jennings, L. K. *et al.* Pel is a cationic exopolysaccharide that cross-links extracellular DNA in the Pseudomonas aeruginosa biofilm matrix. *Proc Natl Acad Sci U S A* **112**, 11353-11358, doi:10.1073/pnas.1503058112 (2015).

23 Kocharova, N. A., Knirel, Y. A., Shashkov, A. S., Kochetkov, N. K. & Pier, B. P. Structure of an Extracellular Cross-reactive Polysaccharide from Pseudomonas aeruginosa Immunotype 4*. *Journal of Biological Chemistry* **263**, 11291-11295 (1988).

24 Borlee, B. R. *et al.* Pseudomonas aeruginosa uses a cyclic-di-GMP-regulated adhesin to reinforce the biofilm extracellular matrix. *Mol Microbiol* **75**, 827-842, doi:10.1111/j.1365-2958.2009.06991.x (2010).

25 Reichhardt, C., Wong, C., Passos da Silva, D., Wozniak, D. J. & Packman, A. I. CdrA Interactions within the Pseudomonas aeruginosa Biofilm Matrix Safeguard It from Proteolysis and Promote Cellular Packing. *Molecular Biology and Physiology* **9**, doi:10.1128/mBio (2018).

26 Adam, J. *et al.* Engineering of PA-IIL lectin from Pseudomonas aeruginosa - Unravelling the role of the specificity loop for sugar preference. *BMC Struct Biol* **7**, 36, doi:10.1186/1472-6807-7-36 (2007).

27 Mitchell, E. P. *et al.* High affinity fucose binding of Pseudomonas aeruginosa lectin PA-IIL: 1.0 A resolution crystal structure of the complex combined with thermodynamics

and computational chemistry approaches. *Proteins* **58**, 735-746, doi:10.1002/prot.20330 (2005).

28 Sabin, C. *et al.* Binding of different monosaccharides by lectin PA-IIL from Pseudomonas aeruginosa: thermodynamics data correlated with X-ray structures. *FEBS Lett* **580**, 982-987, doi:10.1016/j.febslet.2006.01.030 (2006).

29 Adam, E. C., Mitchell, B. S., Schumacher, D. U., Grant, G. & Schumacher, U. Pseudomonas aeruginosa II Lectin Stops Human Cillary Beating: Therapeutic Implications of Fucose. *American Journal of Respiratory Critical Care Medicine* **155**, 2102-2104 (1997).

30 Tielker, D. *et al.* Pseudomonas aeruginosa lectin LecB is located in the outer membrane and is involved in biofilm formation. *Microbiology* **151**, 1313-1323, doi:10.1099/mic.0.27701-0 (2005).

31 Passos da Silva, D. *et al.* The Pseudomonas aeruginosa lectin LecB binds to the exopolysaccharide Psl and stabilizes the biofilm matrix. *Nat Commun* **10**, 2183, doi:10.1038/s41467-019-10201-4 (2019).

32 Su, F. Y. *et al.* Polymer-augmented liposomes enhancing antibiotic delivery against intracellular infections. *Biomater Sci* **6**, 1976-1985, doi:10.1039/c8bm00282g (2018).

33 Das, D. *et al.* Synthetic Macromolecular Antibiotic Platform for Inhalable Therapy against Aerosolized Intracellular Alveolar Infections. *Mol Pharm* **14**, 1988-1997, doi:10.1021/acs.molpharmaceut.7b00093 (2017).

34 Su, F. Y. *et al.* Macrophage-targeted drugamers with enzyme-cleavable linkers deliver high intracellular drug dosing and sustained drug pharmacokinetics against alveolar pulmonary infections. *J Control Release* **287**, 1-11, doi:10.1016/j.jconrel.2018.08.014 (2018).

35 Chen, J., et al. . Glycan targeted polymeric antibiotic prodrugs for alveolar macrophage infections. *Biomaterials*, doi: https://doi.org/10.1016/

a. j.biomaterials.2018.10.017. (2018).

36 Das, D. *et al.* Radiant star nanoparticle prodrugs for the treatment of intracellular alveolar infections. *Polymer Chemistry* **9**, 2134-2146, doi:10.1039/c8py00202a (2018).

37 Christensen, B. B. *et al.* Molecular Tools for Study of Biofilm Physiology. *Methods in Enzymology* **310**, 20-42 (1999).

38 M. Guvenir, A. Arikan, Hepatitis B virus: from diagnosis to treatment, Pol. J. Microbiol. 69 (4) (2020) 391–399, https://doi.org/10.1016/j.patbio.2010.05.002.

4 Acknowledgments

Thanks first to Happy, who accompanied and supported me through these 6 years of graduate school. Your quiet affection and insistent cuddles supported me through the years. Thank you for persevering, fighting with me to the end through my masters defense and to the last word of my thesis before leaving us.

Thanks to my mentor and graduate advisor Dr. Daniel Ratner. Your guidance was fundamental, helping me navigate life at UW and providing helpful suggestions when science failed to science. When I started to question what I do and why I'm doing it, your enthusiasm always helped to reignite the spark of excitement for my research and revived my faith in my work.

Thanks to my duckies, Yuliette Medina, Megan Luu, Megan Allen, and Neona Lowe. It was an honor guiding you through your introduction to lab work, research, and college. Your excitement to learn and grow always inspired my own growth and research. You were excellent mentees and friends.

Thanks to my lab mates, Neona Lowe and Vaishnavi Dhawan, for being so supportive and being such great friends. You filled the lab and office with laughter, particularly when I was editing your applications. I wish you all the success in graduate school!

Thank you to Dr. Eoin West for being on my committee and for your support in my research .

Thank you to all of the collaborators I have worked with throughout the years. Thank you to everyone in the Ratner, Stayton, Skerrett, West, Guttman, CSIRO, and Johnson labs. Thank you to Dr. Patrick Stayton, Dr. Shawn Skerrett, Dr. Eoin West, Dr. Matt Parsek, Dr. Miklos Guttman, Dr. Anthony Convertine, Dr. Jill Johnson, , Dr. Peter Kingshott, Dr. Mrinal Bhave, Dr. Alexander Dart, Dr. Daniel Passos da Silva, Dr. Courtney Reichardt, Dr. Debobrato "Jojo" Das, Dr. Fang-Yi "Ida" Su, Dr. Jasmine Chen, Dr. Selvi Srinivasan, Dr. Vladimir Vlaskin, Dr. Abhigya Mookherjee, Dr. Thomas Chavas, Brian Lee, Dr. Ciana Luisa Lopez, Dr. Ayumi Pottenger, Kerry Lannert, Sanjit Uppal,Caroline Schramm, Lara Lovelace-Macon, and Guilhem F. Reolle. You all helped to make my life and research at UW more colorful, guiding my forays into your fields of expertise. You were the best collaborators I could have asked for.

Thank you to the OWRC and all of my colleagues there, for reminding me that life outside the lab and science exists. Thank you for reminding me that I can make a difference.

Thank you to the EDCs, the ENGR 106 students, and of course, to Dei Caudle, for supporting me during my last two years, for your patience when I struggled. You reinvigorated my excitement to teach, to mentor, and to engineer.

And finally, thank you to my family and friends, for trying to follow along as I babbled about the nuances and technical details of my research, and for your support during the most trying times of graduate school.